

# Investigations of ultrafast nuclear response induced by resonant and nonresonant laser pulses

Anand T. N. Kumar, Florin Rosca, Allan Widom, and Paul M. Champion<sup>a)</sup>

*Department of Physics and Center for Interdisciplinary Research on Complex Systems, Northeastern University, Boston, Massachusetts 02115*

(Received 13 November 2000; accepted 25 January 2001)

We analyze the nonstationary vibrational states prepared by ultrashort laser pulses interacting with a two electronic level molecular system. Fully quantum mechanical expressions are derived for all the moments of the coordinate and momentum operators for the vibrational density matrices associated with the ground and excited electronic states. The analysis presented here provides key information concerning the temperature and carrier frequency dependence of the moments, and relates the moments to equilibrium absorption and dispersion line shapes in a manner analogous to the “transform methods” previously used to describe resonance Raman scattering. Particular attention is focused on the first two moments, for which simple analytical expressions are obtained that are computationally easy to implement. The behavior of the first two moments with respect to various parameters such as the pulse carrier (center) frequency, pulse width, mode frequency, electron-nuclear coupling strength, and temperature is investigated in detail. Using rigorous analytical formulas, we also discuss the laser pulse induced squeezing of the nuclear distributions as well as the pulse induced vibrational heating/cooling in the ground and excited states. The moment analysis of the pump induced state presented here offers a convenient starting point for the analysis of signals measured in pump-probe spectroscopy. The moment analysis can also be used, in general, to better understand the material response following ultrashort laser pulse excitation.

© 2001 American Institute of Physics. [DOI: 10.1063/1.1356011]

## I. INTRODUCTION

Femtosecond laser pulses, with durations shorter than typical nuclear vibrations, are widely used to prepare specific molecular states and study their evolution in real time.<sup>1–22</sup> An example is pump-probe spectroscopy, or femtosecond coherence spectroscopy, where an ultrashort pump laser pulse is used to excite the sample of interest. The subsequent nonstationary response of the medium is monitored by a delayed probe pulse. The effect of a short laser pulse incident on a two electronic level molecular system is to induce nonstationary vibrational states (vibrational coherence) in both the ground and excited electronic levels. Ground state coherence, usually ascribed to impulsive stimulated Raman scattering processes,<sup>4–6</sup> is the dominant contribution in systems with short-lived excited states and for off-resonant excitation.<sup>2,10,11,14,16</sup> Vibrational coherence in the excited state is, however, the dominant contribution for systems that have long-lived excited states.<sup>1,7–9,12,13,19,22</sup>

A common description of pump-probe spectroscopy is based on the third-order susceptibility ( $\chi^3$ ) formalism, which provides a unified view of four-wave mixing spectroscopies.<sup>23–26</sup> The state of the molecular system in-between the pump and probe pulse interactions is, however, not explicit in the  $\chi^3$  formalism.<sup>27</sup> It is often the case that the most interesting part of a pump-probe signal is when the pump and probe pulses are well separated in time, a limit usually termed the well separated pulse (WSP) approxima-

tion. A physical model that treats the pump and probe events separately is therefore very useful. An example is the doorway-window picture,<sup>26</sup> which can be used to represent pump and probe events in terms of Wigner phase space wave packets, and readily enables a semiclassical interpretation of pump-probe experiments.<sup>28–30</sup> Another approach in the well-separated pulse limit is based on a description of the pump induced medium using nonstationary effective linear response functions.<sup>10,25,31–33</sup> We have recently demonstrated the application of an effective linear response approach to pump-probe spectroscopy using a displaced thermal state representation of the pump induced (doorway) density matrix.<sup>27</sup> A key requirement for this representation is a knowledge of the moments of position ( $Q$ ) and momentum ( $P$ ) in the doorway state. A moment analysis of the doorway state is well justified by the fact that the vibrational states prepared by short pulses are highly localized in ( $Q, P$ ) phase space. We thus expect the doorway states to be described adequately by the first few moments. In addition, when the first moments of the doorway state are incorporated into the effective linear response functions, the resulting pump-probe signals are in excellent agreement with the predictions of the third-order response approach,<sup>27</sup> which implicitly incorporates all the moments of the doorway density matrix. In addition to providing an accurate description of pump-probe signals in the well-separated pulse limit, a knowledge of the moments allows a clear physical interpretation of the amplitude and phase profiles observed in pump-probe experiments of nonreactive samples.<sup>27,34</sup>

<sup>a)</sup>Electronic mail: champ@neu.edu

Apart from pump–probe experiments, a fully quantitative understanding of the matter states prepared by short laser pulses can by itself serve as a fruitful exercise. For instance, there has been an increasing interest in using single and multiple laser pulses to control molecular dynamics and to generate optimal vibrational motion.<sup>9,35–38</sup> Numerous theoretical studies have addressed impulsive preparation of molecular states in detail and are usually based on a semiclassical treatment of the laser pulse interaction.<sup>36–40</sup> The advantage of the semiclassical approach is that it provides simple analytical expressions that are valid in the short pulse limit,<sup>36–38</sup> and enables several key insights into the generation and detection of coherent wave packet motion.<sup>39,40</sup> A fully quantum treatment, on the other hand, has usually entailed a direct numerical solution of the Schrödinger equation.<sup>35,37,41</sup>

One of the primary motivations of this work was the interpretation of the observed amplitude and phase profiles in femtosecond pump–probe experiments of myoglobin.<sup>27,34</sup> As mentioned earlier, a fully quantum mechanical evaluation of the moments of the doorway state is key to the effective linear response approach, which substitutes for the computationally more intensive third-order response approach.<sup>27</sup> It is also clear that a precise determination of the first and higher moments of the nonstationary wave packets induced by short pulse excitation is useful in the above-mentioned applications.<sup>9,35–37</sup> In the present work, we consider a two electronic level system with a multimode set of linearly displaced harmonic oscillators, and obtain general expressions for the  $n$ th moments of  $Q$  and  $P$  in the doorway density matrix. The first two moments are studied in detail, and are directly connected to equilibrium absorption and dispersion line shape functions. Because of this connection, absolute scale calculations of the moments are made possible even for complex multimode systems, with only a knowledge of the measured equilibrium absorption cross sections. This approach is analogous to “transform” calculations in resonance Raman scattering.<sup>42–46</sup> In addition, the temperature dependence of the moments is clearly revealed in the calculations presented here, and the results are shown to be in good agreement with earlier treatments based on the impulsive (short pulse) approximation.<sup>36–40</sup>

The general outline of the paper is as follows. In Sec. II, we briefly discuss the background for the present work and discuss the basic expressions involved in a perturbative treatment of the laser pulse interaction. In Sec. III, we calculate the first and second moments of  $Q$  and  $P$  in the ground state density matrix using the general expressions for the  $n$ th moments presented in Appendix A. In Sec. IV, we carry out a similar analysis of the first two moments of the excited state density matrix. In Sec. V, we present simulations to study the behavior of the first two moments of  $Q$  and  $P$  as a function of the laser pulse carrier frequency, pulse width, mode frequency, coupling strength, and temperature.

## II. BACKGROUND

We first briefly review the basic expressions involved in a perturbative treatment of the pump induced density matrix. Consider the interaction of a two electronic level system with the pump laser pulse whose electric field is represented

as  $\mathbf{E}(t)$ . We write the total Hamiltonian as  $\hat{H}(t) = \hat{H}_0 + \hat{H}_I(t)$ , with the free Hamiltonian  $\hat{H}_0$  and the interaction Hamiltonian  $\hat{H}_I$  having the following typical form (in the interaction picture) for a molecular system with two electronic levels:

$$\hat{H}_0 = \begin{pmatrix} \hat{H}_e + \hbar\Omega_v & 0 \\ 0 & \hat{H}_g \end{pmatrix}, \quad (1)$$

$$\hat{H}_I(t) = -\hat{\mu}(t) \cdot \mathbf{E}(t) = -\begin{pmatrix} 0 & \hat{\mu}_{ge}(t) \cdot \mathbf{E}(t) \\ \hat{\mu}_{eg}(t) \cdot \mathbf{E}(t) & 0 \end{pmatrix},$$

where  $\hat{H}_g$  and  $\hat{H}_e = \hat{H}_g + \hat{V}$  are, respectively, the adiabatic Born–Oppenheimer Hamiltonians for the ground and excited electronic states.  $\hat{V}$  is defined as the difference potential that specifies the electron nuclear coupling,  $\hbar\Omega_v$  is the vertical electronic energy gap at the equilibrium position of the ground state, and  $\hat{\mu}(t)$  is the electric dipole moment operator evolving according to the free Hamiltonian  $\hat{H}_0$ . Let  $\hat{\rho}(-\infty)$  denote the initial density matrix of the system before the arrival of the pump fields. The evolution of the density matrix due to the laser pulse interaction can be described by the Liouville equation:<sup>47</sup>

$$i\hbar \frac{\partial \hat{\rho}(t)}{\partial t} = [\hat{H}_I(t), \hat{\rho}(t)]. \quad (2)$$

Equation (2) can be solved for  $\hat{\rho}(t)$  iteratively to various orders in the interaction  $\hat{H}_I(t)$ . For pump–probe calculations, the second-order term is of relevance since it is the lowest order in the pump interaction that can contribute to the signals.<sup>48,49</sup> From Eq. (2), we obtain<sup>27</sup> the following form for the density matrix to second-order in the pump interaction:

$$\hat{\rho}(t) = \hat{\rho}(-\infty) + \left(\frac{i}{\hbar}\right)^2 \int_{-\infty}^t dt_2 \int_{-\infty}^{t_2} dt_1 [\hat{\mu}_k(t_2), [\hat{\mu}_l(t_1), \hat{\rho}(-\infty)]] E_k(t_2) E_l(t_1). \quad (3)$$

Note that we have omitted the first-order term as it is not relevant for a pump–probe calculation. In Eq. (3), the indices  $k$  and  $l$  refer to the vector components and summation over repeated indices is implied. Note that the second-order perturbative term is also referred to in the literature as the density matrix jump<sup>50</sup> and the doorway function.<sup>28,30,51</sup> For well-separated pump and probe pulses, one is interested in the density matrix in Eq. (3) after the pump fields  $E(t)$  have ceased to evolve. As  $t \rightarrow \infty$  in Eq. (3), the interaction picture density matrix becomes time independent, and the time arguments will be dropped in the following development.

If we project the density matrix  $\hat{\rho}$  onto the electronic basis, we obtain the nuclear sub-density matrices for the ground and excited electronic states. Noting that the second-order density matrix in Eq. (3) has no electronic coherences due to the even number of dipole interactions, we may write

$$\hat{\rho} = \hat{\rho}_e |e\rangle\langle e| + \hat{\rho}_g |g\rangle\langle g| = \begin{pmatrix} \hat{\rho}_e & 0 \\ 0 & \hat{\rho}_g \end{pmatrix}. \quad (4)$$

In general, the nuclear subdensity matrices  $\hat{\rho}_g$  and  $\hat{\rho}_e$  may contain off-diagonal elements (vibrational coherence) in the number state representation due to the broad frequency spectrum of an ultrashort laser pulse. The presence of off-diagonal terms reflects the nonstationary nature of  $\hat{\rho}$ , which in general does not commute with  $\hat{H}_0$ . The vibrational coherence translates into time-dependent wave packets in a semiclassical phase space ( $Q, P$ ) Wigner representation of the density matrix.<sup>26,40,52,53</sup> On the other hand, the highly localized nature (in  $Q$  and  $P$ ) of impulsively driven nonstationary states suggests that we calculate their moments in the state  $u$  (which represents  $g$  or  $e$ ) using

$$\bar{X}_u(t) = \text{Tr}[\langle u | \hat{X}(t) | u \rangle \hat{\rho}_u] / \text{Tr}[\hat{\rho}_u]. \quad (5)$$

With  $\hat{a}(\hat{a}^\dagger)$  as the mode annihilation (creation) operators,  $\hat{X}$  represents  $\hat{Q} = (\hat{a} + \hat{a}^\dagger) / \sqrt{2}$ ,  $\hat{P} = i(\hat{a}^\dagger - \hat{a}) / \sqrt{2}$ , or their higher powers. The time  $t$  in Eq. (5) is larger than the pulse duration so that the density matrix  $\hat{\rho}_s$  is time independent. However, the  $t=0$  values<sup>54</sup> of the first moments of  $\hat{Q}$  and  $\hat{P}$ , i.e.,  $\bar{Q}_u(0)$  and  $\bar{P}_u(0)$ , respectively (for  $u=g$  or  $u=e$ ), determine the effective initial conditions for the subsequent nuclear dynamics on the potential surface  $u$ . Since  $\bar{Q}_u(0)$  and  $\bar{P}_u(0)$  also denote shifts from thermal equilibrium, we may represent the nonstationary nuclear density matrix for the electronic state “ $u$ ” as a coherent-thermal state:

$$\hat{\rho}_u = \hat{D}(\lambda_u) \hat{\rho}_T^{(u)} \hat{D}^\dagger(\lambda_u). \quad (6)$$

Here,  $\hat{D}(\lambda_u)$  is the quantum mechanical displacement operator<sup>55</sup>

$$\hat{D}(\lambda_u) = \exp(\lambda_u \hat{a}^\dagger - \lambda_u^* \hat{a}), \quad (7)$$

with  $\lambda_u = (\bar{Q}_u(0) + i\bar{P}_u(0)) / \sqrt{2}$ .  $\hat{\rho}_T^{(u)}$  is the equilibrium thermal density matrix corresponding to the nuclear Hamiltonian of the electronic level  $u$ :

$$\hat{\rho}_T^{(u)} = Z^{-1} \exp(-\hat{H}_u / k_B T). \quad (8)$$

The displaced thermal state representation in Eq. (6) has been shown<sup>27</sup> to provide an accurate and computationally efficient approach to calculating pump–probe signals. This presents us with the primary motivation for a rigorous moment analysis of the pump induced density matrix. As we will see in the following, the laser pulse can induce higher moment changes (also termed squeezing) in the vibrational distributions in addition to merely displacing them. Equation (6) is only an approximation to the full second-order density matrix in Eq. (3). The higher moments of  $\hat{\rho}_u$  calculated here can be incorporated in a manner analogous to Eq. (6) using a displaced and squeezed state representation.

In Appendix A, we derive general expressions for the  $n$ th moments of  $\hat{Q}(t)$  and  $\hat{P}(t)$  for the pump induced nuclear density matrices  $\hat{\rho}_g$  and  $\hat{\rho}_e$  for a two level system, with a single linearly coupled (undamped) mode. In what follows, we discuss the effect of the pump pulse interaction on the vibrational populations and the first two moments of  $\hat{Q}$  and  $\hat{P}$  in the ground and excited states.

### III. NONEQUILIBRIUM GROUND STATE DENSITY MATRIX

For simplicity, we restrict the discussion here to scalar fields assuming that the medium is isotropic. We make the Condon approximation that neglects the nuclear coordinate dependence of the dipole operator and write  $\hat{\mu} = \mu_{ge} |g\rangle\langle e| + \mu_{eg} |e\rangle\langle g|$ . The system is assumed to be initially in the ground electronic state with an equilibrium Boltzmann distribution for the vibrational states, i.e.,  $\hat{\rho}(-\infty) = |g\rangle\hat{\rho}_T^{(g)}\langle g|$ , where  $\hat{\rho}_T^{(g)}$  is of the form in Eq. (8) with  $\hat{H}_s$  replaced by  $\hat{H}_g$ . The ground state density matrix to second order in the pump fields is evaluated using Eq. (3) as  $\hat{\rho}_g = \langle g | \hat{\rho} | g \rangle$ . We find

$$\hat{\rho}_g = \hat{\rho}_T^{(g)} - \frac{|\mu_{ge}|^2}{\hbar^2} \int_{-\infty}^{\infty} dt' \int_0^{\infty} ds E(t') E(t'-s) e^{-\Gamma_{eg}|s|} \times \left\{ e^{-i\Omega_v s} \exp\left(-\frac{i}{\hbar} \int_{t'-s}^{t'} ds' \hat{V}(s')\right) \hat{\rho}_T^{(g)} + \text{h.c.} \right\}, \quad (9)$$

where the subscript (+) denotes time ordering and h.c. denotes Hermitian conjugate. We have defined  $s = t' - t''$  for convenience.  $\hat{V}(s)$  evolves in time via  $\hat{H}_g$  in the interaction picture. We have also introduced homogeneous broadening using the factor  $e^{-\Gamma_{eg}|s|}$  to account for electronic dephasing processes. It is evident from Eq. (9) that the action of the electron-nuclear coupling force (which appears through the time-ordered exponential) on the equilibrium state  $\hat{\rho}_T^{(g)}$  resembles a square wave pulse interaction that turns on and off at times separated by an interval  $s$ . The total effect of the pulse on the ground state is obtained by a superposition of square wave interactions for all possible time intervals within the duration of the pump pulse.

Equation (9) is valid for arbitrary ground and excited state nuclear Hamiltonians. In what follows we consider a model of linearly displaced harmonic oscillators for the ground and excited states and take  $\hat{V} = -(\hbar/m\omega_0)^{1/2} f \hat{Q} = -\hbar\omega_0 \Delta \hat{Q}$ , with dimensionless  $\hat{Q}$  and relative displacement  $\Delta$ . The electron-nuclear coupling force  $f$  is expressed as  $f = \Delta(m\omega_0^3 \hbar)^{1/2}$  where  $m$  and  $\omega_0$  are, respectively, the reduced mass and frequency of the mode. With these definitions, the ground and excited state Hamiltonians take the form

$$\hat{H}_g = \frac{\hbar\omega_0}{2} [\hat{Q}^2 + \hat{P}^2], \quad (10a)$$

$$\hat{H}_e = \frac{\hbar\omega_0}{2} [(\hat{Q} - \Delta)^2 + \hat{P}^2] - \frac{\hbar\omega_0 \Delta^2}{2}. \quad (10b)$$

#### A. Populations

The pump pulse induces a net change in the ground and excited electronic state populations, which is reflected in the zeroth moment, i.e., the trace of the respective nuclear density matrices. The electronic population in the ground state after the pump pulse interaction is calculated as  $\mathcal{N}_g = \text{Tr}[\hat{\rho}_g]$ . Using Eq. (9), we find,

$$\mathcal{N}_g = 1 - \frac{|\mu_{ge}|^2}{\hbar^2} \int_{-\infty}^{\infty} dt' \int_0^{\infty} ds E(t') E(t'-s) \times \{e^{-i\Omega_{00}s} e^{-g(s)} e^{-\Gamma_{eg}|s|} + \text{c.c.}\}, \quad (11)$$

where  $\Omega_{00} = \Omega_v - \omega_0 \Delta^2/2$  is the zero-zero electronic transition frequency and  $g(s)$  is the harmonic oscillator correlation function. For a single undamped mode,

$$g(s) = (\Delta^2/2)[(\bar{n}+1)(1-e^{-i\omega_0 s}) + \bar{n}(1-e^{i\omega_0 s})], \quad (12)$$

with  $\bar{n} = (\exp(\hbar\omega_0/k_B T) - 1)^{-1}$ . Analytic expressions for  $g(s)$  for the damped harmonic oscillator case at arbitrary temperature have been derived earlier<sup>56</sup> and can be incorporated in the expressions derived in this work. In terms of the Fourier transform  $\tilde{E}(\omega)$  of the electric field, Eq. (11) takes the form

$$\mathcal{N}_g = 1 - \frac{|\mu_{ge}|^2}{\pi\hbar^2} \int_{-\infty}^{\infty} d\omega |\tilde{E}(\omega)|^2 \Phi_I(\omega), \quad (13)$$

where  $\Phi_I(\omega)$  is the imaginary part of the complex equilibrium line shape function defined as

$$\Phi(\omega) = i \int_0^{\infty} ds e^{i(\omega - \Omega_{00})s} e^{-\Gamma_{eg}|s|} e^{-g(s)}. \quad (14)$$

The imaginary part of the line shape function is directly related to the absorption cross section as  $\sigma_A(\omega) = (8\pi|\mu_{ge}|^2/3\hbar c)\omega\Phi_I(\omega)$ . We take the electric field to be of the form  $E(t) = E_0 G(t) \cos(\omega_c t)$  where  $G(t)$  is a dimensionless Gaussian envelope function. The corresponding Fourier transform is then  $\tilde{E}(\omega) = E_0[\tilde{G}(\omega - \omega_c) + \tilde{G}(\omega + \omega_c)]/2$  where  $\tilde{G}(\omega)$  is the Fourier transform of  $G(t)$ . When this definition is used in Eq. (13), four terms result from the expansion of  $\tilde{E}^2(\omega)$ . Equation (13) contains contributions from the line shape function at negative frequencies, i.e.,  $\Phi_I(\omega < 0)$ . It is clear that the integrand in Eq. (14) is highly nonresonant for  $\omega < 0$ , so that the line shape function makes a vanishing contribution at negative frequencies. Thus, we neglect those terms in Eq. (13) that contain the negative frequency part of the pulse envelope spectrum, i.e.,  $\tilde{G}(\omega + \omega_c)$  and take only the positive frequency part of the integral in Eq. (13). This is a valid (“rotating wave”) approximation, given that we are concerned with pulses that have optical carrier frequencies. We then arrive at the following result:

$$\mathcal{N}_g = 1 - \frac{|\mu_{ge}|^2 E_0^2}{4\pi\hbar^2} \int_0^{\infty} d\omega \tilde{G}^2(\omega - \omega_c) \Phi_I(\omega). \quad (15)$$

The depletion in the net ground electronic state population thus depends on the convolution of the laser intensity spectrum with the absorption line shape as one would expect. Since the total number of molecules must be conserved (neglecting decay through other nonradiative channels during the pump pulse), the corresponding number of molecules transported to the excited state by the pump is simply given by  $\mathcal{N}_e = 1 - \mathcal{N}_g$ . It should be remembered that Eq. (15) has been derived in the weak field perturbative limit and the number of molecules depleted from the ground state is very small (i.e.,  $\mathcal{N}_g \approx 1$ ).

The line shape function  $\Phi(\omega)$  plays a central role throughout the calculations presented in this work. While the electronic populations depend only on the imaginary part of  $\Phi(\omega)$ , we will see in the following that the moments of  $\hat{Q}$  and  $\hat{P}$  in the pump induced nonequilibrium density matrix involve both the absorptive and dispersive line shapes  $\Phi_I(\omega)$  and  $\Phi_R(\omega)$ .

## B. Vibrational dynamics

The interaction with the laser pulse sets up both electronic and vibrational coherence in the system. However, the electronic coherence vanishes for a second-order interaction with the pump laser field, owing to the even dipole interactions in the second-order perturbative expression for the density matrix in Eq. (3). We therefore focus attention on the vibrational coherence induced in the electronic states.

### 1. First moment

The first moment of  $\hat{Q}(t)$  in the ground state is obtained by letting  $n = 1$  in the general expression Eq. (A10). We find

$$\bar{Q}_g(t) = \frac{1}{2i\mathcal{N}_g} \sum_{l=0}^{\infty} \sum_{m=0}^{\infty} \delta_{1,2l+m} \frac{(-1)^{l+m}}{l!m!} \Delta^m (2\bar{n}+1)^l \times [\mathcal{C}_m(t) + (-1)^m \mathcal{C}_m^*(t)], \quad (16)$$

where  $\mathcal{C}_m(t)$  is given by Eq. (A11). Due to the Kronecker's delta, we must have  $l=0$  and  $m=1$ , so that

$$\bar{Q}_g(t) = -(\Delta/\mathcal{N}_g) \text{Im}[\mathcal{C}_1(t)]. \quad (17)$$

Using Eqs. (A11) and (A9), we find

$$\mathcal{C}_1(t) = \frac{|\mu_{ge}|^2}{2\pi\hbar^2} \int_{-\infty}^{\infty} d\omega \tilde{E}(\omega) \{(\bar{n}_T+1)e^{-i\omega_0 t} \tilde{E}^*(\omega - \omega_0) \times [\Phi(\omega) - \Phi(\omega - \omega_0)] - \bar{n}_T e^{i\omega_0 t} \tilde{E}^*(\omega + \omega_0) \times [\Phi(\omega) - \Phi(\omega + \omega_0)]\}. \quad (18)$$

Equation (18) again involves nonresonant contributions from the line shape function at negative frequencies, i.e.,  $\Phi(\omega < 0)$ . For pulses with optical carrier frequencies, the contribution of the negative frequency components is negligible and can be dropped from the above integral. We then find, after making a change of variables  $\omega \rightarrow \omega - \omega_0$  in the second part of the above integral and using the definition of  $\tilde{E}(\omega)$  following Eq. (12),

$$\bar{Q}_g(t) = |A_{1g}| \cos(\omega_0 t + \varphi_{1g}), \quad (19)$$

where  $A_{1g} = \bar{Q}_g(0) + i\bar{P}_g(0) = |A_{1g}| \exp(-i\varphi_{1g})$  is the complex amplitude for first moment dynamics in the ground state, with the effective “initial” position and momentum  $\bar{Q}_g(0)$  and  $\bar{P}_g(0)$  given by:

$$\bar{Q}_g(0) = -\frac{|\mu_{ge}|^2 E_0^2 (2\bar{n}+1) \Delta}{8\pi\hbar^2 \mathcal{N}_g} \times \int_0^{\infty} d\omega \tilde{G}_p(\omega - \omega_c, -\omega_0) \hat{\Delta} \Phi_I(\omega), \quad (20a)$$

$$\bar{P}_g(0) = \frac{|\mu_{ge}|^2 E_0^2 \Delta}{8\pi\hbar^2 \mathcal{N}_g} \int_0^\infty d\omega \tilde{G}_p(\omega - \omega_c, -\omega_0) \hat{\Delta} \Phi_R(\omega). \quad (20b)$$

Here, we have introduced the product spectral function  $\tilde{G}_p(\omega, n\omega_0)$ :

$$\tilde{G}_p(\omega, n\omega_0) = \tilde{G}(\omega) \tilde{G}(\omega + n\omega_0), \quad (21)$$

and the difference operator  $\hat{\Delta}$  (not to be confused with the dimensionless coupling  $\Delta$ ) whose action is to generate differences as<sup>46</sup>

$$\hat{\Delta} \Phi_I(\omega) = \Phi_I(\omega) - \Phi_I(\omega - \omega_0), \quad (22a)$$

$$\begin{aligned} \hat{\Delta}^2 \Phi_I(\omega) &= \hat{\Delta} [\Phi_I(\omega) - \Phi_I(\omega - \omega_0)] \\ &= \Phi_I(\omega) - 2\Phi_I(\omega - \omega_0) + \Phi_I(\omega - 2\omega_0), \end{aligned} \quad (22b)$$

and so on for the higher powers of  $\hat{\Delta}$ .

Equations (20a) and (20b) are fully quantum mechanical expressions for the first moments and are valid for arbitrary pulse widths, temperature, and electron-nuclear displacement  $\Delta$ . It is clear that the mean initial position and momentum imparted by the pump pulse to the ground state wave packet are related roughly to the derivatives of the imaginary and real parts of the equilibrium line shape function, respectively. In Appendix B, we discuss the impulsive limit of the above-mentioned results and also present a closed form expression for the mean position assuming a Gaussian (semi-classical) form for  $\Phi_I(\omega)$ . The single mode expressions in Eqs. (20a) and (20b) can be readily generalized to the multimode case, with the same equations applying for a given mode with parameters  $\omega_i$ ,  $\Delta_i$ , and  $\bar{n}_i$ . The line shapes can be obtained using the multimode form of the equilibrium correlation function in Eq. (12). In fact, Eqs. (20a) and (20b) (as well as the rest of the moment expressions derived in this work) are quite general multimode expressions so long as the mode of interest is linearly coupled and  $\Phi(\omega)$  is obtained from the experimental line shape. In this case, the remaining multimode subspace resides in the experimental line shape function, unrestricted by approximations such as linear coupling and mode mixing.

## 2. Second moment

In addition to the first moments of the nuclear position and momentum, it is also of interest to calculate the pump induced changes in the variances (or the uncertainties) of the position and momentum distributions. Before the interaction with the laser fields, the position and momentum uncertainties (defined in terms of the variances  $\sigma_A^2 = \bar{A}^2 - \bar{A}^2$ , with  $A = Q, P$ ) have equal values at temperature  $T$ :

$$\sigma_Q = \sigma_P = \sqrt{\bar{n} + 1/2}. \quad (23)$$

The effect of the pump pulse is to distort the equilibrium nuclear distributions and modify the above-given variances. To see what is involved, we express  $\hat{Q}$  and  $\hat{P}$  in terms of  $\hat{a}$  and  $\hat{a}^\dagger$  using the definitions following Eq. (5) and obtain the second moment of  $\hat{Q}(t)$  in the pump induced ground state as:

$$\begin{aligned} \overline{Q}_g^2(t) &= (1/2\mathcal{N}_g) \text{Tr}[\hat{\rho}_g(\hat{a}^2(t) + \hat{a}^{\dagger 2}(t) + \hat{a}^\dagger \hat{a} + \hat{a} \hat{a}^\dagger)] \\ &= \bar{n}_g + 1/2 + |A_{2g}| \cos(2\omega_0 t + \varphi_{2g}), \end{aligned} \quad (24)$$

where we have also used  $\hat{a}(t) = \hat{a} e^{-i\omega_0 t}$ . The quantities  $\bar{n}_g$  and  $A_{2g} = |A_{2g}| \exp(-i\varphi_{2g})$  are, respectively, the mean value of the number operator  $\hat{n} = \hat{a}^\dagger \hat{a}$  and the mean value of  $\hat{a}^2$ , for the state described by  $\hat{\rho}_g$ . It is clear from Eq. (24) that the second moment in the pump induced state consists of both vibrational coherence at frequency  $2\omega_0$  and the mean occupation number of the ground state. The amplitude of the second moment dynamics at frequency  $2\omega_0$  is given by  $|A_{2g}|$ . If  $\overline{Q}_g^2(t) - \overline{Q}_g(t)^2$  is time-dependent, the nuclear distribution has been squeezed by the laser pulse interaction.<sup>57-60</sup> In what follows, we evaluate  $\overline{Q}_g^2(t)$  using the general result Eq. (A10), which assumes the second-order perturbative expression for  $\hat{\rho}_g$  given in Eq. (9). A direct comparison of the results with the identity in Eq. (24) subsequently leads to expressions for  $\bar{n}_g$  and  $A_{2g}$  to second-order in the fields.

If we set  $n=2$  in Eq. (A10), the allowed sets of values of  $(l, m)$  are (1,0) and (0,2) and we find

$$\overline{Q}_g^2(t) = \frac{2\bar{n} + 1}{2\mathcal{N}_g} (1 + 2 \text{Re}[C_0(t)]) - \frac{\Delta^2}{2\mathcal{N}_g} \text{Re}[C_2(t)]. \quad (25)$$

Using Eqs. (A11) and (15) we have  $\text{Re}[C_0(t)] = (\mathcal{N}_g - 1)/2$ . The quantity  $C_2(t)$  is also readily evaluated using Eq. (A11). On comparing the final result with Eq. (24) and ignoring nonresonant contributions, the second-order expressions for mean occupation number and the oscillatory amplitude of the second moment are found as

$$\begin{aligned} \bar{n}_g &= \bar{n} - \frac{|\mu_{ge}|^2 E_0^2 \Delta^2 \bar{n} (\bar{n} + 1)}{8\pi\hbar^2 \mathcal{N}_g} \\ &\quad \times \int_0^\infty d\omega \tilde{G}^2(\omega - \omega_c) \hat{\Delta}^2 \Phi_I(\omega + \omega_0), \quad (26) \\ A_{2g} &= - \frac{|\mu_{ge}|^2 E_0^2 \Delta^2}{8\pi\hbar^2 \mathcal{N}_g} \int_0^\infty d\omega \tilde{G}_p(\omega - \omega_c, -2\omega_0) \\ &\quad \times [(\bar{n}^2 + \bar{n} + 1/2) \hat{\Delta}^2 \Phi_I(\omega) - i(\bar{n} + 1/2) \hat{\Delta}^2 \Phi_R(\omega)]. \end{aligned} \quad (27)$$

As discussed in Appendix A, the second moment of the momentum operator is obtained as  $\overline{P}_g^2(t) = \overline{Q}_g^2(t + \pi/2\omega_0)$ , so that

$$\overline{P}_g^2(t) = \bar{n}_g + 1/2 - |A_{2g}| \cos(2\omega_0 t + \varphi_{2g}). \quad (28)$$

The variances of  $\hat{Q}$  and  $\hat{P}$  in the pump induced ground state can be directly obtained using Eqs. (24) and (28) along with the first moments  $\overline{Q}_g(t)$  and  $\overline{P}_g(t)$  given by Eq. (19). For the time-dependent uncertainty product, we find

$$\begin{aligned} \sigma_{Qg}(t) \sigma_{Pg}(t) &\cong \bar{n}_g + \frac{1}{2} (1 - |A_{1g}|^2) - \frac{|A_{2g}|^2}{(2\bar{n}_g + 1)} \\ &\quad \times \cos^2(2\omega_0 t + \varphi_{2g}). \end{aligned} \quad (29)$$

In obtaining Eq. (29), small terms involving higher powers of the electric field strength have been ignored, since we are in the weak field limit. Furthermore, in typical weak coupling situations,  $|A_{2g}|$  is much smaller than  $|A_{1g}|$  since it scales with the square of the coupling strength  $\Delta$ . Thus, the time-dependent term of Eq. (29) is very small and the uncertainty product is nearly time independent.

A direct inspection of Eqs. (26) and (27) reveals an apparent contradiction. When the system is initially at  $T=0$ , we have  $\bar{n}_g=0$ , i.e., there is no change in the vibrational populations due to the pump-pulse interaction. The oscillatory amplitudes  $A_{1g}$  and  $A_{2g}$  that describe the ground state coherence are, however, not necessarily vanishing at  $T=0$ , as evident from Eqs. (27) and (20a) and (20b). The number basis elements of  $\hat{\rho}_g$  therefore obey the following relations:

$$(\hat{\rho}_g)_{0j} \neq 0, \quad (\hat{\rho}_g)_{00} = 1, \quad (\hat{\rho}_g)_{jj} = 0, \quad \forall j \neq 0, \quad (30)$$

in violation of the density matrix inequality condition<sup>61</sup>  $|\rho_{ij}|^2 \leq \rho_{ii}\rho_{jj}$  for any given pair of vibrational levels  $i$  and  $j$ . Thus, strictly speaking,  $\hat{\rho}_g$  is *not* a complete vibrational density matrix.<sup>40</sup> Furthermore, we have from Eqs. (26) to (29), at  $T=0$ ,

$$\sigma_{Q_g}(0)\sigma_{P_g}(0) \equiv \frac{1}{2}(1 - |A_{1g}|^2), \quad (31)$$

which is always less than the zero point limit of 1/2. These apparent discrepancies are due to the second-order perturbative approximation to the full density matrix employed here as well as elsewhere.<sup>29,30,32,37,38,50</sup> A genuine change in the vibrational populations in the ground state can only occur due to a fourth-order interaction, via stimulated Raman scattering processes. Thus, the complete expressions for the second moments of the pump induced density matrix would necessitate the inclusion of fourth-order terms in the perturbation expansion. This is beyond the scope of the present paper. However, we can estimate the magnitude of the error in the calculation to be roughly  $|A_{1g}|^2$  [from Eq. (31)], which goes as the fourth power of the electric field strength and is typically very small for weak fields. We will return to a discussion of this issue in Sec. V, where we also present a quantitative estimate for the error made in a second-order perturbative treatment for a simple model system.

#### IV. NONEQUILIBRIUM EXCITED STATE DENSITY MATRIX

The excited state density matrix is obtained from Eq. (3) as  $\hat{\rho}_e = \langle e | \hat{\rho} | e \rangle$ . Here, the terms with a single dipole interaction on either side of  $\hat{\rho}_T$  in the expression for  $\hat{\rho}$  will contribute. For the linear displaced Hamiltonians in Eqs. (10a) and (10b), we find

$$\begin{aligned} \hat{\rho}_e = & \frac{|\mu_{ge}|^2}{\hbar^2} \int_{-\infty}^{\infty} dt' \int_{-\infty}^{t'} dt'' E(t')E(t'') \\ & \times \left\{ \exp(i\Omega_{vs} - \Gamma_{eg}|s|) \left( \exp\left(-i\omega_0\Delta \int_0^{t'} ds' \hat{Q}(s')\right) \right) \right\}_- \\ & \times \hat{\rho}_T^{(g)} \left( \exp\left(i\omega_0\Delta \int_0^{t''} ds' \hat{Q}(s')\right) \right)_+ + \text{h.c.} \end{aligned} \quad (32)$$

where the subscript  $-$  denotes anti-time ordering.

#### A. Populations

The fraction of excited state molecules  $\mathcal{N}_e$  is simply  $\mathcal{N}_e = 1 - \mathcal{N}_g$  as the sum of the ground and excited state populations must be conserved (ignoring other channels for the decay of the excited state). We thus have from Eq. (15),

$$\mathcal{N}_e = (|\mu_{ge}|^2 E_0^2 / 4\pi\hbar^2) \int_0^{\infty} d\omega \tilde{G}^2(\omega - \omega_c) \Phi_I(\omega). \quad (33)$$

In the weak field approximation assumed here,  $\mathcal{N}_e \ll 1$ . Thus, only a small fraction of the ground state is transported to the excited state by the pump interaction.

#### B. Vibrational dynamics

##### 1. First moment

In Appendix B, we calculate the moments of the shifted coordinate operator  $\hat{Q}'_e(t) = \hat{Q}_e(t) - \Delta$  for the excited state density matrix (the subscript  $e$  indicates time evolution due to  $\hat{H}_e$ ). The first moment is obtained by letting  $n=1$  in Eq. (A21). Only the term with  $(l=0, m=1)$  contributes and we find

$$\overline{Q}'_e(t) = -(\Delta/\mathcal{N}_e) \text{Im}[\mathcal{D}_1(t)]. \quad (34)$$

From Eqs. (A22) and (A19), we find after neglecting non-resonant contributions,

$$\overline{Q}'_e(t) = |A_{1e}| \cos(\omega_0 t + \varphi_{1e}), \quad (35)$$

where  $A_{1e} = \overline{Q}'_e(0) + i\overline{P}_e(0) = |A_{1e}| \exp(-i\varphi_{1e})$  is the amplitude for the first moment dynamics (about the equilibrium position  $\Delta$ ) in the excited state, with the effective initial position and momentum given by

$$\begin{aligned} \overline{Q}'_e(0) = & -\frac{|\mu_{ge}|^2 E_0^2 \Delta}{4\pi\hbar^2 \mathcal{N}_e} \int_0^{\infty} d\omega \tilde{G}_p(\omega - \omega_c, -\omega_0) \\ & \times [\Phi_I(\omega - \omega_0) - \bar{n} \hat{\Delta} \Phi_I(\omega)], \end{aligned} \quad (36a)$$

$$\overline{P}_e(0) = 0. \quad (36b)$$

Thus, the excited state wave packet receives no initial momentum. Correspondingly, the initial phase  $\varphi_{1e}$  can only take the values 0 or  $\pi$ . Note that Eq. (35) gives the time-dependent mean position with respect to the excited state equilibrium position  $\Delta$ . To revert to the ground state equilibrium as the origin, we simply write

$$\overline{Q}_e(t) = \Delta + |A_{1e}| \cos(\omega_0 t + \varphi_{1e}). \quad (37)$$

The absence of initial momentum on the excited state wave packet might be expected on intuitive grounds. The vibrational modes that are formed in the excited electronic state are subject to the electron-nuclear coupling force that turns on (during the pump interaction) and thereafter, remains a constant. Thus, the forces on excited state nuclei are step function-like. In contrast, the ground state nuclei feel the electron-nuclear coupling force only for a short time during the pulse interaction, so that the forces on the ground state

are impulsive in nature. It is interesting to note that Eq. (36b) is predicted by earlier treatments that use the semiclassical Franck approximation,<sup>51,62</sup> where more general potentials were treated than the harmonic approximation made in the present case. It is also notable from Eq. (36a) that in sharp contrast to the ground state case, the excited state first moment involves only the imaginary part of the line shape function  $\Phi_I(\omega)$ . This difference reflects the fact that the ground state coherence is created by Raman-type processes. It is well known<sup>42,43,46</sup> that the resonance Raman cross section involves both the real and imaginary parts of the line shape function. The excited state coherence is created solely by absorption-like events occurring on the bra and ket sides of the density matrix as expressed in Eq. (32).

### 2. Second moment

From the definitions in Eqs. (A13) and (A12), we have  $\hat{Q}'_e(t) = (\hat{a}_e e^{-i\omega_0 t} + \hat{a}_e^\dagger e^{i\omega_0 t})/\sqrt{2}$  so that the following general relation holds analogous to Eq. (24):

$$\overline{Q_e'^2}(t) = \bar{n}_e + 1/2 + |A_{2e}| \cos(2\omega_0 t + \varphi_{2e}), \quad (38)$$

where  $\bar{n}_e$  is the mean value of the occupation number  $\hat{n}_e = \hat{a}_e^\dagger \hat{a}_e$ , and  $A_{2e} = |A_{2e}| e^{-i\varphi_{2e}}$  is the mean value of  $\hat{a}^2$  in the pump induced excited state. If we let  $n=2$  in the general expression derived in Eq. (A21), the allowed sets of values for  $(l, m)$  are  $(1, 0)$  and  $(0, 2)$  and we get

$$\overline{Q_e'^2}(t) = \frac{2\bar{n}_e + 1}{\mathcal{N}_e} \text{Re}[\mathcal{D}_0(t)] - \frac{\Delta^2}{2\mathcal{N}_e} \text{Re}[\mathcal{D}_2(t)]. \quad (39)$$

Using Eq. (A22) we have  $\text{Re}[\mathcal{D}_0(t)] = \mathcal{N}_e/2$ . The quantity  $\text{Re}[\mathcal{D}_2(t)]$  is also evaluated readily using Eq. (A22). Comparing the final result with Eq. (38), we find that the mean occupation number of the pump induced excited state oscillator  $\bar{n}_e$  is given by

$$\bar{n}_e = \bar{n} - \bar{n}(\bar{n} + 1)\Delta^2 + \frac{|\mu_{ge}|^2 E_0^2 \Delta^2}{8\pi\hbar^2 \mathcal{N}_e} \int_0^\infty d\omega \tilde{G}^2(\omega - \omega_c) \times [(\bar{n} + 1)^2 \Phi_I(\omega - \omega_0) + \bar{n}^2 \Phi_I(\omega + \omega_0)]. \quad (40)$$

The oscillatory amplitude is given by

$$A_{2e} = (|\mu_{ge}|^2 E_0^2 \Delta^2 / 8\pi\hbar^2 \mathcal{N}_e) \times \int_0^\infty d\omega \tilde{G}(\omega - \omega_c + \omega_0) \tilde{G}(\omega - \omega_c - \omega_0) \Phi'(\omega), \quad (41)$$

where we have defined the function

$$\Phi'(\omega) = [\Phi_I(\omega - \omega_0) - 2\bar{n}\hat{\Delta}\Phi_I(\omega) + \bar{n}^2\hat{\Delta}^2\Phi_I(\omega + \omega_0)]. \quad (42)$$

The amplitude  $A_{2e}$  for the second moment dynamics at frequency  $2\omega_0$  is real so that the phase  $\varphi_{2e}$  can take on only the values 0 or  $\pi$ . This is in contrast to the ground state results derived in Sec. III B 2. Both the first and the second moments in the excited state depend only on the absorptive line shape

function  $\Phi_I(\omega)$  whereas the ground state moments depend on both  $\Phi_I(\omega)$  and  $\Phi_R(\omega)$ .

The second moment of the momentum operator is obtained as before by letting  $t \rightarrow t + \pi/2\omega_0$  in  $\overline{Q_e'^2}(t)$ . The first moment and the second moment results can be combined to obtain the uncertainties in  $\hat{Q}$  and  $\hat{P}$ . For the position uncertainty, we find

$$\sigma_{Q_e}(t) = [\bar{n}_e + (1 - A_{1e}^2)/2 + (A_{2e} - A_{1e}^2/2)\cos(2\omega_0 t)]^{1/2}. \quad (43)$$

The momentum uncertainty is obtained as  $\sigma_{P_e}(t) = \sigma_{Q_e}(t + \pi/2\omega_0)$ . For the time-dependent uncertainty product, we get

$$\sigma_{Q_e}(t)\sigma_{P_e}(t) \cong \bar{n}_e + \frac{1}{2}(1 - A_{1e}^2) - \frac{A_{2e}(A_{2e} - A_{1e}^2)}{(2\bar{n}_e + 1)} \times \cos^2(2\omega_0 t), \quad (44)$$

where we have neglected terms that contain powers of  $A_{1e}$  and  $A_{2e}$  larger than second, since they involve higher powers of the field strength  $E_0$ , which is assumed to be very weak. Equation (44) is simpler than Eq. (29) for the ground state due to the lack of an initial phase for the excited state first and second moments. Once again, for weak electron-nuclear coupling, the uncertainty product is nearly time independent, since  $A_{2e}$  is typically much smaller than  $A_{1e}$ .

We note from the above-given expressions that the second-order density matrix  $\hat{\rho}_e$  is not in explicit violation of the uncertainty principle as is the pump induced ground state density  $\hat{\rho}_g$ . To see this clearly, we first note from Eqs. (36a) and (33) that at  $T=0$ ,  $|A_{1e}| \leq \Delta$  since  $\tilde{G}_p(\omega - \omega_c, -\omega_0) \leq \tilde{G}(\omega - \omega_c)$ . Also, from Eq. (40), we have  $\bar{n}_e \cong \Delta^2/2$ , provided the vibrational frequency can be neglected in  $\Phi_I(\omega \pm \omega_0)$  (a condition known as ultrafast electronic dephasing<sup>26</sup>). It then follows from Eq. (44) that at  $T=0$ ,

$$\sigma_{Q_e}(t)\sigma_{P_e}(t) \cong 1/2, \quad (45)$$

where the error in Eq. (45) is to fourth order in the field strength and is very small for weak fields. Thus, the second-order approximation to the excited state density matrix is more accurate than for the ground state density matrix. This difference is not surprising, given that a change in the vibrational populations of the excited state can be effectively induced by a second-order interaction. This stands in contrast to the ground state vibrational levels, where the populations change due to scattering processes via a fourth-order interaction.

### V. SIMULATIONS AND DISCUSSION

For the simulations reported here, fast Fourier transforms were employed to calculate the complex line shape function in Eq. (14), for a given set of model parameters. The precalculated line shape functions are subsequently used in all the moment calculations, thereby reducing the computation time significantly. The single integration in the moment expressions is computationally straightforward, as the integrands are smooth functions that are highly convergent (owing to the Gaussian spectral envelope of the laser pulse).

In this section, we investigate the behavior of the ground and excited state moments as a function of various parameters such as the pulse carrier frequency, temperature, mode frequency, coupling strength, and pulse duration.

One attractive feature of the moment expressions derived in this work is that apart from parameters specific to the mode under consideration, all other information about the rest of the modes (and the bath) is carried through in the equilibrium line shape functions  $\Phi_I$  and  $\Phi_R$ . These are not independent quantities but are rather connected by the Kramers–Kronig relations. One can therefore obtain  $\Phi_I(\omega)$  directly from the measured experimental absorption cross section (on an absolute scale). The Kramers–Kronig relations can then be used to obtain  $\Phi_R(\omega)$  from  $\Phi_I(\omega)$ . Thus, given a molecule in the condensed phase whose absorption spectrum is known experimentally (and is possibly broad and asymmetric), one can use the results derived here to calculate the moments of the pulse induced nonequilibrium state on an absolute scale, for any given mode of the system. Furthermore, since the relation between moments and  $\Phi_I(\omega)$ ,  $\Phi_R(\omega)$  is linear, we can also extend the main results derived in this paper to account for inhomogeneous broadening due to a distribution of electronic 0–0 transition frequencies.<sup>63</sup>

## A. First moments

### 1. Ground state

Consider the ground state first moments of  $\hat{Q}$  and  $\hat{P}$  derived in Eqs. (20a) and (20b). Several interesting features are evident from a direct inspection of these expressions. When the carrier frequency of the pump pulse  $\omega_c$  is tuned across the resonant maximum ( $\Omega_v$ ),  $\bar{Q}_g(0)$  changes sign owing to its dependence on the derivative-like function  $\hat{\Delta}\Phi_I(\omega)$ . It is also clear from Eq. (20a) that for detuning to the red of the absorption band,  $\bar{Q}_g(0)$  has a sign opposite to that of  $\Delta$ , while it has the same sign as  $\Delta$  for blue detuning. The dependence of  $\bar{P}_g(0)$  on  $\hat{\Delta}\Phi_R(\omega)$  implies that in the region of resonance, the momentum impulse is oppositely directed with respect to the electron-nuclear coupling force  $f$ . Also, the sign of  $\bar{P}_g(0)$  changes as we tune away from resonance on either side of  $\Omega_v$ . When the pulse carrier frequency is detuned far from the resonant transition (but neglect of the nonresonant terms remains valid),  $\hat{\Delta}\Phi_I(\omega)$  drops more rapidly to zero when compared with  $\hat{\Delta}\Phi_R(\omega)$  so that  $\bar{Q}_g(0)$  is much smaller than  $\bar{P}_g(0)$ . Thus, for off-resonant excitation, the ground state coherence is dominated by a momentum impulse. Under off-resonant excitation, Eq. (20b) implies that  $\bar{P}_g(0)$  has the same sign as  $\Delta$  and therefore points in the same direction as the electron-nuclear coupling force. The well known off-resonant impulsive limit<sup>15</sup> is thus seen to arise from the dependence of the momentum impulse on the derivative of the real part of the line shape function.<sup>39</sup> The fully quantum mechanical treatment further shows that the approach to the off-resonant limit depends strongly on the temperature and mode frequency, as we will see in the following. The distinct dependence of  $\bar{Q}_g(0)$  and  $\bar{P}_g(0)$  on temperature ( $T$ ) is also noted from Eqs. (20a)–(20b). While the  $T$  dependence of  $\bar{Q}_g(0)$  is determined both by the factor

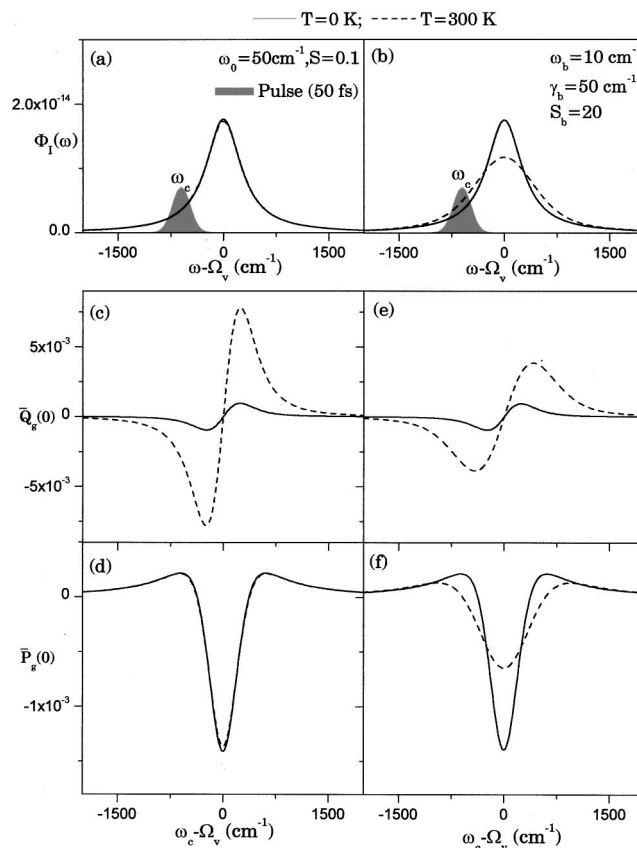


FIG. 1. Temperature and carrier frequency dependence of the mean nuclear position and momentum in the pump induced ground state. (a) Absorption line shape function  $\Phi_I(\omega)$  for a homogeneously broadened system ( $\Gamma_{eg} = 300 \text{ cm}^{-1}$ ) consisting of a single linearly coupled mode ( $\omega_0 = 50 \text{ cm}^{-1}$ ,  $S = 0.1$ ). The solid line shows  $\Phi_I(\omega)$  for  $T = 0 \text{ K}$  and the dashed line for  $T = 300 \text{ K}$ . (b) Same as in (a) but with an additional overdamped bath mode ( $\omega_b = 10 \text{ cm}^{-1}$ ,  $S_b = 20$ ,  $\gamma_b = 50 \text{ cm}^{-1}$ ) included in the line shape. (c) and (d) The pump pulse induced effective initial position and momentum in the ground state (in dimensionless units) for the  $50 \text{ cm}^{-1}$  mode, for both line shapes in (a). (e) and (f) The mean position and momentum for the strongly temperature-dependent line shape in (b). For all the simulations, a Gaussian with full width at half maximum of 50 fs was used for the electric field, and the total pulse energy was fixed at 1 nJ.

$(2\bar{n} + 1)$  and the line shape  $\Phi_I(\omega)$ ,  $\bar{P}_g(0)$  depends on  $T$  solely through the real part of the line shape function  $\Phi_R(\omega)$ .

In order to illustrate the above-mentioned aspects of the ground state first moments, we consider two model line shapes. In the first example, shown in the left panel of Fig. 1, a low frequency mode [ $\omega_0 = 50 \text{ cm}^{-1}$ ,  $S = (\Delta^2/2) = 0.1$ ] is coupled to a homogeneously broadened ( $\Gamma_{eg} = 300 \text{ cm}^{-1}$ ) two level system. Figure 1(a) shows the imaginary part of line shape function at two different temperatures. The corresponding mean position and momentum for the  $50 \text{ cm}^{-1}$  mode are shown in the panels directly below, for a range of  $\omega_c$  values across the resonance maximum. The pulse width is chosen to be 50 fs. The second example, shown in the right panel of Fig. 1, consists of a line shape that is strongly temperature dependent due to the presence of a strongly coupled overdamped bath mode in addition to the  $50 \text{ cm}^{-1}$  mode. Vibrational damping was incorporated<sup>64</sup> using a rigorous theory presented previously.<sup>56</sup>

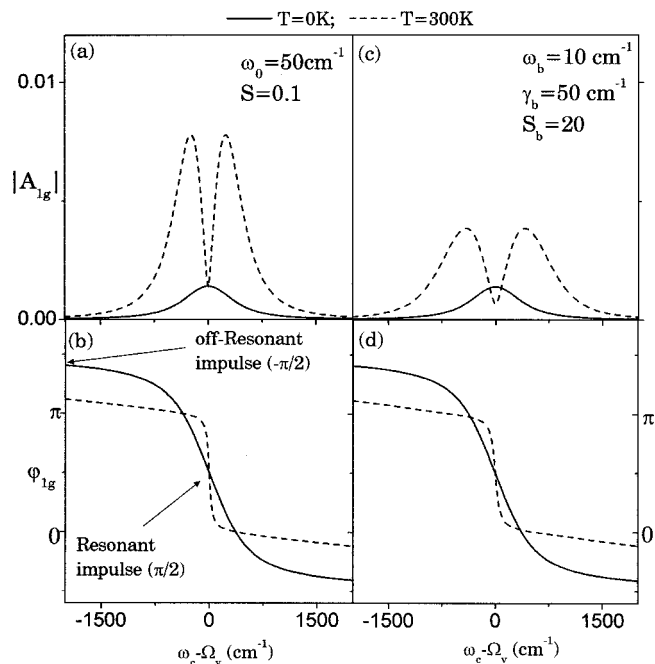


FIG. 2. The first moment amplitude  $|A_{1g}|$  and phase  $\varphi_{1g}$  for the  $50 \text{ cm}^{-1}$  mode in the pump induced ground state, plotted for both line shapes considered in Fig. 1. (a) and (b)  $|A_{1g}|$  and  $\varphi_{1g}$  for the Lorentzian line shape in Fig. 1(a) and (c) and (d) for the phonon broadened line shape in Fig. 1(b). The solid lines correspond to  $T=1 \text{ K}$  and the dashed lines correspond to  $T=300 \text{ K}$ .

From the simulations, it is seen that some of the general features evident from a direct inspection of Eqs. (20a) and (20b) are borne out; note in particular, the behavior of the position and momentum as roughly the derivatives of the absorptive and dispersive line shapes. Thus, the momentum increment is peaked at absorption maximum  $\Omega_v$  and is directed opposite to the excited state equilibrium shift, which in the present case is positive. The position increment is peaked at roughly the full width at half maximum of the absorption, and changes sign as the carrier frequency is tuned across  $\Omega_v$ . The difference in the temperature dependence of the position and momentum increments is also clear. It is seen that for the weakly temperature-dependent line shape, the momentum increment is nearly unaffected by temperature changes, while the position increment increases dramatically owing to the Bose–Einstein factor. The situation is different for the strongly temperature-dependent line shape, in which case, it is seen that the momentum imparted to the wave packet changes significantly with temperature, with a decreased value at the  $\Omega_v$  [corresponding to the fact that  $\Phi_R(\omega)$  is broader at higher temperature, which in turn implies that the derivative is smaller]. It is also interesting to note the behavior as  $\omega_c$  is tuned away from resonance, where it is seen that  $\bar{Q}_g(0)$  approaches zero while  $\bar{P}_g(0)$  still has a nonzero value.

The relative magnitudes of  $\bar{Q}_g(0)$  and  $\bar{P}_g(0)$  are best understood by plotting the amplitude and phase of the wave packet motion defined in Eq. (19). In Fig. 2, we plot the initial amplitude and phase of the pump induced wave packet as a function of the pulse carrier frequency for both examples considered in Fig. 1. It is seen from the phase plot (lower

panels) that at high temperatures (larger  $\bar{n}$ ) the phase remains close to 0 or  $\pi$ . When the temperature is lowered, the phase varies more continuously over a range of  $2\pi$ . This corresponds to the fact that the position increment [real part of the complex displacement,  $A_{1g} = \bar{Q}_g(0) + i\bar{P}_g(0)$ ] dominates the momentum increment (imaginary part) at high temperatures, except at resonant maximum  $\Omega_v$ . Furthermore, when the pump is tuned to  $\Omega_v$ , the purely impulsive ( $\bar{Q}_g(0) = 0 \Rightarrow \varphi_g = \pi/2$ ) nature of the ground state coherence is evident. As the pump carrier frequency is tuned toward the off-resonance limit, the phase is again seen to approach the impulsive limit ( $\varphi_g = -\pi/2$ ), and this approach occurs much more rapidly at lower temperatures than high. This is again owing to the fact that the high temperature case is dominated by the position increment. Note that the momentum imparted to the ground state wave packet by resonant and nonresonant pulses are opposite in direction, with the momentum of a resonantly induced wave packet directed opposite to the electron nuclear coupling force.

Several of the above-mentioned aspects of detuning dependence of  $\bar{Q}_g(0)$  and  $\bar{P}_g(0)$  have been noted in earlier semiclassical treatments.<sup>36–40</sup> The results for the excitation frequency dependence of the ground state first moments are in qualitative agreement with the predictions of Cina and co-workers,<sup>37</sup> who have used semiclassical pulse propagators to study the impulsive preparation of ground state nuclear motion due to single and multiple laser pulse excitation. Their calculations suggest that excitation in the preresonant region induces much larger increments in the nuclear position than excitation directly on resonance. From the present work, this aspect directly follows from the dependence of the position increment on the derivative of the absorption line shape function as expressed in Eq. (20a). We also note that semiclassical models have been used to show that the ground state momentum impulse depends on the derivative of the real part of polarizability.<sup>39</sup> The present fully quantum mechanical treatment clearly exposes the distinct temperature dependence of the pulse induced position and momentum in the ground state. While the temperature dependence is not included explicitly in prior treatments, more complicated potential surfaces have been analyzed. But the general nature of the pump induced position and momentum predicted here for harmonic potentials remains valid.

## 2. Excited state

Turning to the excited state first moment, recall from Sec. IV that the wave packet created in the excited state receives no initial momentum. As mentioned earlier, the lack of initial momentum for the excited state wave packet can be attributed to the step function-like nature of the forces felt by the nuclei of excited state molecules. This argument is expected to be valid for more complicated potentials than the harmonic model considered here. This is indeed the case as shown by earlier treatments.<sup>51</sup> On the other hand, the ground state nuclei are subject to an impulsive square wave force. This results in a nonzero average initial momentum of the ground state wave packet.

Consider the initial displacement of the excited state wave packet  $\bar{Q}'_e(0)$  in Eq. (36a). The temperature dependence of  $\bar{Q}'_e(0)$  is mainly determined by the factor  $\bar{n}$ , which appears as the coefficient of the derivative-like  $\hat{\Delta}\Phi_I(\omega)$ . At zero temperature, or for temperatures low enough so that  $\bar{n} \ll 1$ , all the terms in the integrand of Eq. (36a) are positive. Thus, the overall sign of  $\bar{Q}'_e(0)$  is always opposite to that of  $\Delta$ , irrespective of other parameters such as the laser pulse width and carrier frequency. This leads us to the following interesting conclusion: when the laser pulse interacts with a system that is initially at  $T=0$  (or with negligible thermal population  $\bar{n}$ ), the wave packet created in the excited state is always placed initially on the side of the excited state potential well that lies toward the ground state equilibrium. In other words, the initial phase  $\varphi_{1e}$  of the excited state first moment dynamics is always fixed at 0 or  $\pi$ , depending only on the sign potential displacement  $\Delta$ . As the temperature is increased, the difference term  $\hat{\Delta}\Phi_I(\omega)$  that appears as the coefficient of  $\bar{n}$  in Eq. (36a) begins to remove the positivity of the integrand, since the difference  $\Phi_I(\omega) - \Phi_I(\omega - \omega_0)$  can take on either positive or negative values. However, for line shapes that are broad compared to the vibrational frequency,  $\hat{\Delta}\Phi_I(\omega)$  is still quite small compared to  $\Phi_I(\omega)$  and the derivative term dominates only at very high temperatures (when  $\bar{n} \gg 1$ ).

We take the model line shape treated in Fig. 1(a) to illustrate key aspects of the excited state first moment. In Fig. 3, we plot the excited state first moments for the 50  $\text{cm}^{-1}$  mode. In addition to the amplitude of oscillations  $|A_{1e}| = |\bar{Q}'_e(0)|$  about the excited state equilibrium, the initial value of the first moment with respect to the ground state equilibrium  $\bar{Q}_e(0)$  [see Eq. (37)] is also plotted for clarity. We note that in contrast to the ground state amplitude [Fig. 2(a)], the sign of the temperature-dependent changes in the excited state amplitude depends on the direction of the carrier frequency detuning from the absorption maximum. It is seen that for red detuning from absorption maximum,  $|A_{1e}|$  decreases with increase in temperature, whereas for blue detuning, the amplitude increases with temperature. This opposite behavior on the red and blue sides of the absorption maximum can be understood from the ‘‘particle-like’’ aspect of the excited state coherence, which is complementary to the ‘‘holelike’’ nature of the ground state coherence.<sup>40,52</sup> We will return to this point briefly. As is clear from Fig. 3,  $\bar{Q}_e(0)$  changes its sign with respect to the ground state equilibrium position as  $\omega_c$  is tuned across resonance, but its absolute magnitude remains less than  $|\Delta|$ . As the temperature is increased, the derivative line shape in Eq. (36a) becomes more significant due to larger  $\bar{n}$ . The antisymmetry of the amplitude profile with respect to  $\Omega_v$  becomes more pronounced so that excitation toward the blue side induces larger displacements than red excitation.

We note from Figs. 1(c) and 3(a) that the mean positions for the ground and excited state are oppositely signed with respect to the ground state equilibrium. This behavior is related to the particle- versus hole-like nature of the excited and ground state nuclear wave packets. In Fig. 4, we sche-

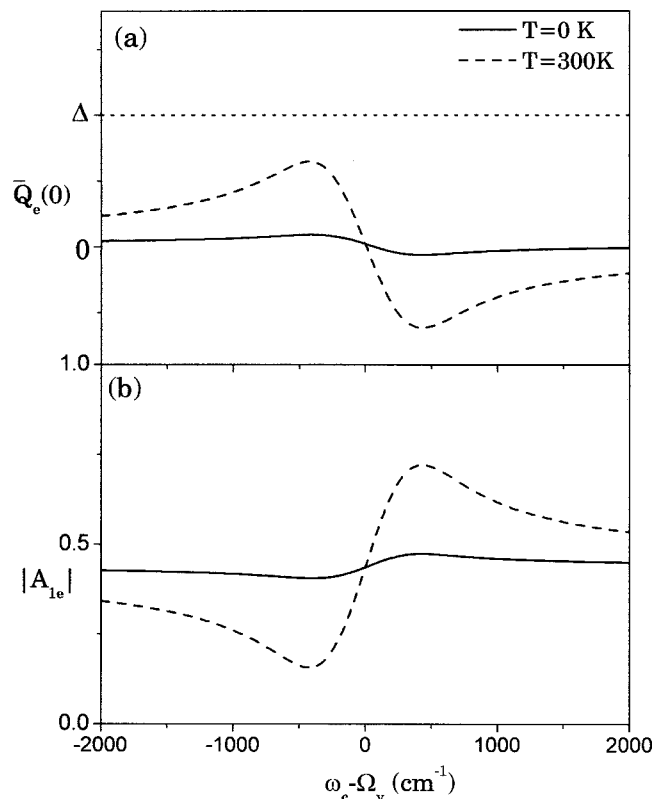


FIG. 3. Temperature and carrier frequency dependence of excited state first moment for the 50  $\text{cm}^{-1}$  mode of the example in Fig. 1(a). The effective initial ( $t=0$ ) mean position  $\bar{Q}_e(0) = \Delta + \bar{Q}'_e(0)$  is plotted in (a). The momentum in the excited state is vanishing and is not shown. (b) The amplitude  $|A_{1e}| = |\bar{Q}'_e(0)|$  of the oscillatory motion about the excited state equilibrium position  $\Delta$ .

matically depict the impulsively excited nuclear wave packet in the ground and excited states, for the carrier frequency tuned to three different values across the absorption maximum  $\Omega_v$ . Consider the case when the laser pulse carrier frequency is

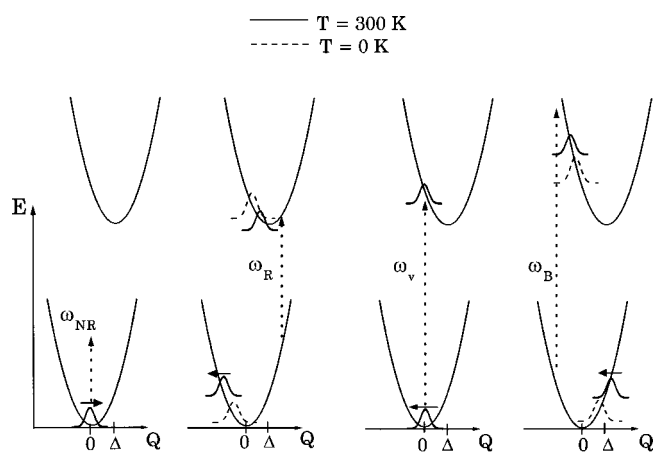


FIG. 4. Schematic of the initial conditions prepared in the ground and excited states of a two-electronic level system, by an impulsive pump interaction. The ground and excited state wave packets are depicted for three different values of the pump carrier frequency as it is tuned across the resonant maximum  $\Omega_v$  and for off-resonant excitation ( $\omega_{NR}$ ). The dotted line indicates the carrier frequency of the laser pulse. The arrows above the ground state wave packets indicate the direction of the initial momentum  $\bar{P}_g(0)$ .

tuned toward the red side of the absorption maximum ( $\omega_R$ ). The pump creates a hole in the ground state near the region of resonance, which is toward positive displacements. The nuclear distribution is therefore effectively centered at negative displacements [i.e.,  $\bar{Q}_g(0) < 0$ ] with respect to equilibrium. The excited state nuclear distribution is, however, created directly near the region of resonance, and is centered at positive displacements. It should be remembered that the normalized mean position of the excited state wave packet [Eq. (36a)] is much bigger than that of the ground state wave packet [Eq. (24)], since  $N_e = 1 - N_g \ll 1$ . The schematic drawn in Fig. 4 merely expresses the opposite signage of the ground and excited state first moments, but does not represent their magnitudes.

It is important to recognize that the schematic shown in Fig. 4 is strictly valid *only in the impulsive approximation*, i.e., when the pulses are much shorter than a vibrational period. In this case, the nuclei of the ground and excited state molecules do not have the time to evolve in their respective surfaces within the duration of the pulse. Thus, one can picture the particle in the excited state as being instantaneously created on the same side of the well where the corresponding hole is created in the ground state. However, when the pulses have a duration that is not too short compared to the vibrational period, the wave packets evolve during the pulse interaction. The centroids of the ground and excited state wave packets are thus no longer expected to be located on opposite sides of the ground state equilibrium. In order to quantify the impulsive limit, it is useful to calculate the population weighted sum of the ground and excited state first moments. Using Eqs. (19) and (37), we arrive at

$$\begin{aligned} N_e \bar{Q}_e(0) + N_g \bar{Q}_g(0) = & - \frac{|\mu_{ge}|^2 E_0^2 \Delta}{8 \pi \hbar^2} \int_0^\infty d\omega \Phi_I(\omega) \\ & \times \bar{G}(\omega - \omega_c) (\Delta^2 \bar{G}(\omega - \omega_c + \omega_0)). \end{aligned} \quad (46)$$

The right-hand side of Eq. (46) is an integral over the second difference of the pulse spectrum. It can be taken to be a small quantity in the impulsive limit, where the spectral bandwidth of the pulse is broad compared to the vibrational frequency. Thus, we may set the right-hand side of Eq. (46) to zero in the impulsive limit. This in turn implies that  $\bar{Q}_e(0) \propto -\bar{Q}_g(0)$ ; i.e., the mean position of the ground and excited state nuclear wave packets are situated on opposite sides of the ground state equilibrium position. This situation holds only for modes with vibrational period much longer than the pulse duration. For longer pulses, the right-hand side of Eq. (46) becomes appreciable. In Fig. 5, we plot the ground and excited state first moments for the  $50 \text{ cm}^{-1}$  mode of the previous example, and the sum defined in Eq. (46), for three different pulse widths. It is seen that the ground and excited state first moments are oppositely signed for the impulsive excitation. However,  $\bar{Q}_e(0)$  and  $\bar{Q}_g(0)$  are no longer symmetric when the pulse duration approaches three quarters of the vibrational period. In this case,  $\bar{Q}_e(0)$  is positive, i.e., the

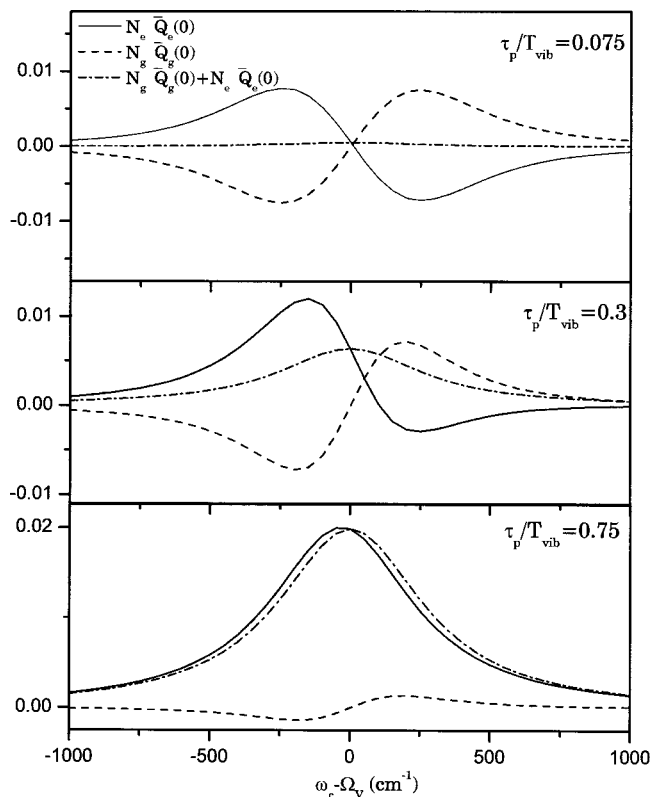


FIG. 5. Study of the symmetry of the ground and excited state mean positions as a function of the pulse width. The population weighted ground and the excited state first moments  $N_g \bar{Q}_g(0)$  and  $N_e \bar{Q}_e(0)$  for the  $50 \text{ cm}^{-1}$  mode (with period  $T_{\text{vib}} \sim 666 \text{ fs}$ ) of the example in Fig. 1(a) are plotted along with their sum, for three different pulse widths. The top panel corresponds to a pulse width  $\tau_p = 50 \text{ fs}$ , middle panel  $\tau_p = 200 \text{ fs}$ , and the bottom panel is with  $\tau_p = 500 \text{ fs}$ .

excited state wave packet is situated to the right of the ground state equilibrium position for the entire range of carrier frequencies plotted.

The relationship  $\bar{Q}_e(0) \propto -\bar{Q}_g(0)$ , which is valid in the impulsive limit, can be used to understand the increase in the asymmetry of the excited state amplitude profile with temperature, as observed in Fig. 3(b). As we have seen earlier,  $\bar{Q}_g(0)$  approaches zero as the temperature is lowered. This means that according to the inverse relation  $\bar{Q}_e(0) \propto -\bar{Q}_g(0)$ , the displacement of the excited state wave packet also approaches 0, but from the opposite side of the equilibrium position as the ground state wave packet. For example, consider the schematic depicted in Fig. 4, where  $\bar{Q}_e(0) > 0$  for excitation toward the red ( $\omega_c = \omega_R$ ). The corresponding approach of  $\bar{Q}_e(0)$  toward zero at low temperatures implies an increase in the amplitude of oscillations about the shifted equilibrium position  $\Delta$ . This is shown by the dashed wave packet in Fig. 4. On the other hand, it is clear that for excitation toward the blue ( $\omega_c = \omega_B$ ), the centroid of the excited state wave packet approaches zero from the negative side of the ground state equilibrium as the temperature is lowered. This corresponds to a wave packet with decreased amplitude of oscillations about the excited state equilibrium, as shown by the dashed wave packet in Fig. 4. Thus the ground and excited state first moments exhibit a

striking contrast in the temperature dependence that can potentially be used to assign the origin of vibrational coherence in pump-probe spectroscopy.<sup>27</sup>

It is clear from the above-mentioned illustrative examples that the analytic expressions for the first moments presented in Eqs. (20a) and (20b) and (36a) expose the temperature and carrier frequency dependence of the first moments. They also offer a physically intuitive picture of the initial conditions prepared by the pump pulse. The accuracy of the first moment expressions is verified by calculations of the pump-probe signals using these expressions in the displaced state representation of the doorway state in Eq. (3). The resulting signals agree well with those calculated using the full third-order response approach.<sup>27</sup> We also note that the depiction of pump induced wave packets in Fig. 4 contradicts prior predictions arising from time-dependent wave packet pictures of impulsive stimulated light scattering. These pictures suggest that the ground state wave packet is always created toward decreasing energy gaps.<sup>10,65,66</sup> However, the analysis presented here as well as in other works<sup>37,38,62</sup> shows that the ground state wave packet induced by impulsive excitation is strongly sensitive to the carrier frequency of the laser pulse.

### 3. Multimode case

The above-considered examples illustrate some of the key aspects of impulsively driven ground and excited state coherence for simple systems with a bath and a single optically coupled mode. As discussed earlier, the expressions derived for the single-mode case can be readily extended to multimode systems. As an example, we consider a two-mode system consisting of a low frequency mode at  $50\text{ cm}^{-1}$  and a high frequency mode at  $220\text{ cm}^{-1}$  coupled to a homogeneously broadened two electronic level system. An overdamped low frequency bath mode is also included to broaden the line shapes. The absorption line shape at  $T=300\text{ K}$  is plotted in Fig. 6(a), and is nearly a Gaussian owing to the semiclassical limit of strong coupling and high temperature. In the lower panels of Fig. 6, we plot the first moments of the 50 and  $220\text{ cm}^{-1}$  modes in the ground state, assuming a pulse width of 50 fs. Along with the fully quantum mechanical results for the mean position and momentum, amplitude and phase for the two modes, we also plot (for comparison) the analytic result for the mean position in Eq. (B7), valid in the impulsive and semiclassical (Gaussian) approximations.

From the simulations, we once again see the role played by thermal factor ( $\bar{n}$ ) in determining the amplitude and phase behavior. The high frequency mode (smaller  $\bar{n}$ ) exhibits a larger proportion of the momentum than the low frequency mode (larger  $\bar{n}$ ). Note that for the chosen pulse duration of 50 fs, the low frequency oscillator (period  $\sim 666$  fs) is driven by the laser pulse in the impulsive limit. The high frequency mode (period  $\sim 150$  fs) is, however, dynamic even during the pulse interaction and is far from being impulsively driven. As would be expected, the agreement of the analytic result for impulsive excitation in Eq. (B7) with the fully quantum expression in Eq. (20a) is much better for the low frequency  $50\text{ cm}^{-1}$  mode than for the higher frequency  $220\text{ cm}^{-1}$

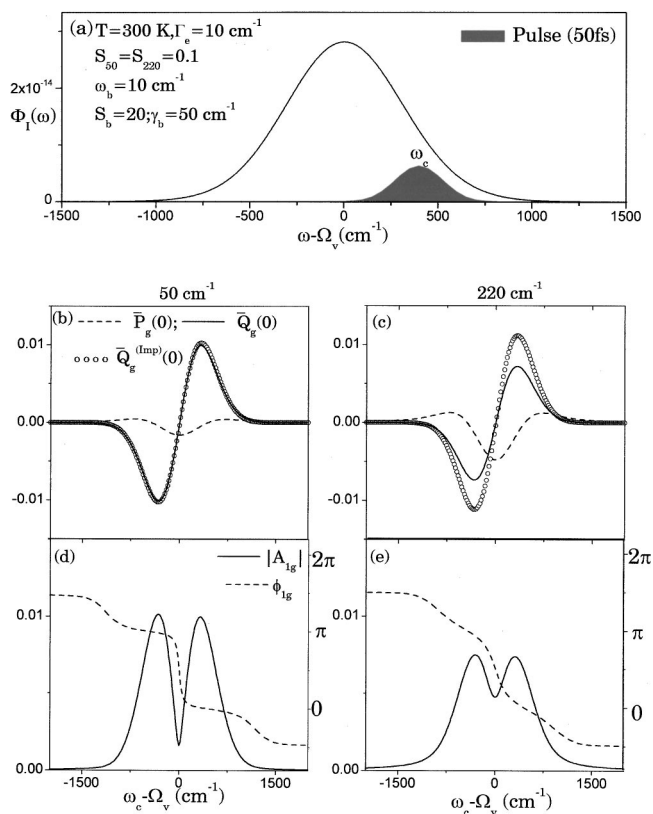


FIG. 6. (a) Absorption line shape at  $T=300\text{ K}$  for a three-mode system consisting of a strongly coupled overdamped bath mode ( $\omega_b=10\text{ cm}^{-1}$ ,  $S_b=20$ ,  $\gamma_b=50\text{ cm}^{-1}$ ) and two other modes with parameters ( $\omega_1=50\text{ cm}^{-1}$ ,  $S_1=0.1$ ) and ( $\omega_2=220\text{ cm}^{-1}$ ,  $S_2=0.1$ ). The homogeneous damping is  $\Gamma_{eg}=10\text{ cm}^{-1}$ . (b) and (c) The pulse induced mean position (solid line) and the mean momentum (dashed line), along with the analytic expression for mean position calculated in the impulsive approximation in Eq. (B7) (circles). (d) and (e) The amplitude and phase of the 50 and  $220\text{ cm}^{-1}$  modes.

mode. While much of the earlier work on this subject<sup>36,38,67,68</sup> has been carried out assuming vibrationally abrupt pulses, we see that a more complete treatment that accounts for the finite pulse width is essential in a multimode situation.

### B. Second moments

Apart from inducing vibrational coherence (off-diagonal terms), the laser pulse also induces changes in the vibrational populations. In Secs. III B 2 and IV B 2, we presented expressions for the second moments of the coordinate and momentum, as well as the pulse induced change in the mean occupation number in the ground and excited states. It is of interest to calculate the pulse induced changes in the variances of the ground and excited state nuclear distributions. The variances of  $Q$  and  $P$  reflect the pulse induced squeezing of the vibrational wave packet, as well as the vibrational heating and cooling in the ground and excited states by the laser pulse. Squeezing of the ground state and excited state wave packets can contribute to overtone signals in pump-probe spectroscopy.<sup>27</sup> In the present section, we discuss some aspects of pulse induced position and momentum uncertainties for a simple model system.

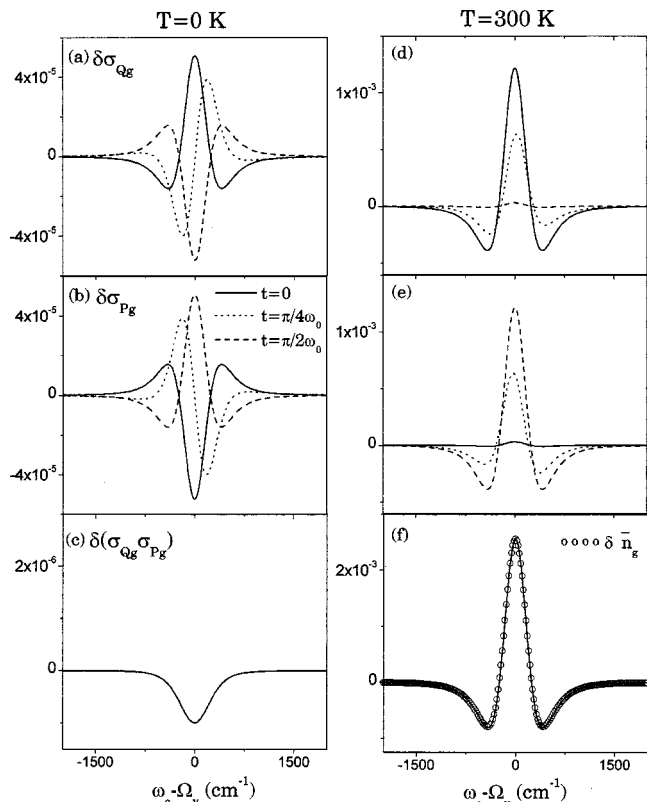


FIG. 7. Temperature and carrier frequency dependence of the position and momentum uncertainties in the pulse induced ground state vibrational distribution. The pulse induced changes (from the thermal equilibrium values) in the position uncertainty  $\delta\sigma_Q$ , momentum uncertainty  $\delta\sigma_P$ , and their product  $\delta(\sigma_Q\sigma_P)$  are plotted at times  $t=0$  (solid line),  $t=\pi/4\omega_0$  (dotted line), and  $t=\pi/2\omega_0$  (dashed line). (a)–(c)  $\delta\sigma_{Qg}$ ,  $\delta\sigma_{Pg}$ , and  $\delta(\sigma_{Qg}\sigma_{Pg})$  at  $T=0$  K. (d)–(f) The corresponding quantities at  $T=300$  K.

We first consider the ground state second moments. As discussed following Eq. (24), the second moments of  $Q$  and  $P$  involve both the diagonal and off-diagonal density matrix elements. The diagonal elements (which are time independent as long as there is no coupling of the mode to an external bath) give rise to a constant width in the coordinate and momentum distributions. The off-diagonal terms give rise to squeezing dynamics at twice the vibrational frequency. From Eq. (27), we note that the real and imaginary parts of the second moment amplitude  $A_{2g}$  are related roughly to the second derivative of the absorptive and dispersive line shape functions  $\hat{\Delta}^2\Phi_I(\omega)$  and  $\hat{\Delta}^2\Phi_R(\omega)$ . The temperature dependence of the real and imaginary parts of  $A_{2g}$  are mainly governed by the factors  $\bar{n}^2 + \bar{n} + 1/2$  and  $\bar{n} + 1/2$ , respectively. Thus, the phase  $\varphi_{2g}$  of the second moment dynamics is strongly dependent on temperature and carrier frequency. At zero temperature, the real and imaginary parts are comparable in magnitude, whereas for high temperatures such that  $\bar{n}^2 \gg \bar{n}$ , the real part of  $A_{2g}$  dominates. This situation is similar to the first moment, where the mean position (real part) dominates the momentum (imaginary part) at high temperatures.

In Fig. 7, we consider the  $50\text{ cm}^{-1}$  mode of the model system in Fig. 1(a), and study the temperature and carrier frequency dependence of the pulse induced position and mo-

mentum uncertainties. Since the pulse induced changes in the variances are very small, it is convenient to plot the differences of various quantities from the thermal equilibrium values, i.e.,  $\delta\sigma_{Qg} = \sigma_{Qg} - \sqrt{\bar{n} + 1/2}$ ,  $\delta\sigma_{Pg} = \sigma_{Pg} - \sqrt{\bar{n} + 1/2}$  and  $\delta(\sigma_{Qg}\sigma_{Pg}) = \sigma_{Qg}\sigma_{Pg} - (\bar{n} + 1/2)$ . We plot  $\delta\sigma_{Qg}$  and  $\delta\sigma_{Pg}$  for a range of carrier frequencies across the absorption spectrum, at three different times during a half-period  $\pi/2\omega_0$  of the second moment dynamics at frequency  $2\omega_0$ . We see that at  $t=0$ ,  $\delta\sigma_{Qg}$  mimics the second derivative of the absorptive line shape owing to its dependence on  $\hat{\Delta}^2\Phi_I(\omega)$ . At  $t = \pi/4\omega_0$  (which is a quarter period of the overtone dynamics at  $2\omega_0$ ) the dispersive term  $\hat{\Delta}^2\Phi_R(\omega)$  dominates. The absorptive and dispersive line shapes thus act in quadrature to determine the overall dynamics of  $\sigma_{Qg}(t)$ , which is thus strongly sensitive to the carrier frequency detuning from the absorption maximum. According to the relation  $\sigma_{Pg}(t) = \sigma_{Qg}(t + \pi/2\omega_0)$ , the momentum uncertainty simply ‘lags’ the position uncertainty by  $1/4$  vibrational period, as shown in Fig. 7(b). The position momentum uncertainty product is plotted in Fig. 7(c) and is independent of time. Note the small dip of the uncertainty product below the vacuum product of one-half, which arises from the term  $|A_{1g}|^2$  in Eq. (29). As discussed following Eq. (29), this unphysical behavior is attributed to the neglect of fourth-order interactions in the present treatment. While the inclusion of higher order interactions is beyond the scope of the present paper, we can roughly say that the magnitude of the dip, given by  $|A_{1g}|^2$ , effectively estimates the error due to the second-order perturbative approximation made in Eq. (9).

At higher temperature, the mean occupation number  $\bar{n}_g$  dominates the expression for the position and momentum uncertainties. As discussed previously, the variances of  $Q$  and  $P$  at high temperatures are mainly determined by the absorptive function  $\hat{\Delta}^2\Phi_I(\omega)$ , which is the real part of  $A_{2g}$ . This is evident from Figs. 7(d) and 7(e), where the role played by the dispersive term is insignificant compared to the absorptive part. Also, note the increase of the uncertainties by nearly two orders of magnitude relative to the low temperature case. The uncertainty product, shown in Fig. 7(f), once again remains constant with time. The error term  $|A_{1g}|^2$  in Eq. (29) is far less significant compared to  $\bar{n}_g$  at high temperature, and we have  $\sigma_{Qg}\sigma_{Pg} \cong \bar{n}_g + 1/2$ . Indeed, Fig. 7(f) simply reflects the behavior of  $\delta\bar{n}_g = \bar{n}_g - \bar{n}$  calculated in Eq. (26), which is also shown in the figure for comparison. There is a spread in both  $\sigma_{Qg}$  and  $\sigma_{Pg}$  near the absorption maximum, corresponding to pulse induced heating. Near the wings of the absorption spectrum, however, both  $\sigma_{Qg}$  and  $\sigma_{Pg}$  are narrowed from their equilibrium values, corresponding to a laser pulse induced cooling of the ground state.

Turning to the second moments of the excited state wave packet, we recall from Sec. IV that the excited state moments only involve the absorptive line shape function  $\Phi_I(\omega)$ . From Eq. (43) we see that the position uncertainty oscillates (at frequency  $2\omega_0$ ) between  $(\bar{n}_e + 1/2 + A_{2e} - A_{1e}^2)^{1/2}$  at  $t=0$  and  $(\bar{n}_e + 1/2 - A_{2e})^{1/2}$  at  $t = \pi/2\omega_0$ . The momentum uncertainty lags the position uncertainty by  $\pi/2\omega_0$ . In Fig. 8, we depict the detailed behavior of the position and momentum

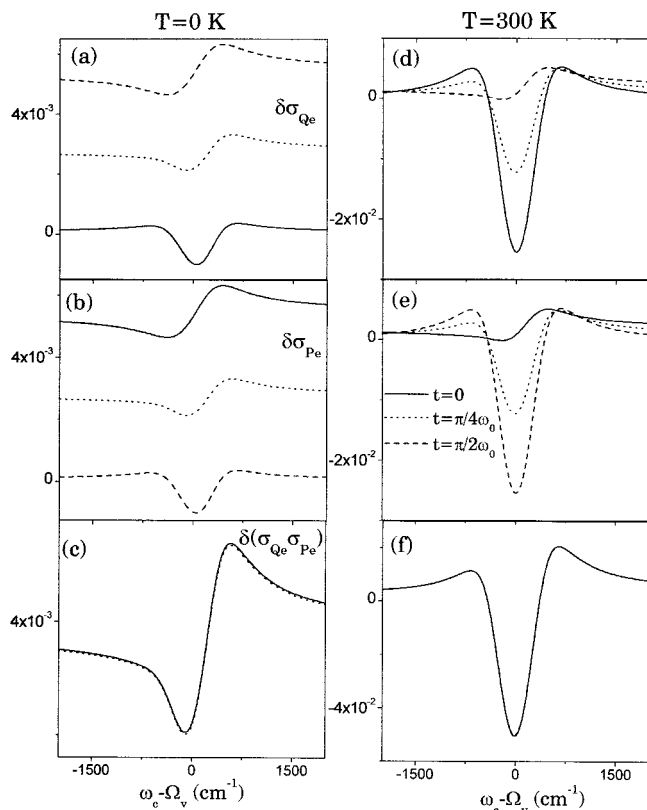


FIG. 8. Temperature and carrier frequency dependence of the position and momentum uncertainties in the pulse induced excited state vibrational distribution. The pulse induced changes (from thermal equilibrium values) in the position uncertainty  $\delta\sigma_{Q_e}$ , momentum uncertainty  $\delta\sigma_{P_e}$ , and their product  $\delta(\sigma_{Q_e}\sigma_{P_e})$  are plotted at times  $t=0$  (solid line),  $t=\pi/4\omega_0$  (dotted line), and  $t=\pi/2\omega_0$  (dashed line). (a)–(c)  $\delta\sigma_{Q_e}$ ,  $\delta\sigma_{P_e}$ , and  $\delta(\sigma_{Q_e}\sigma_{P_e})$  at  $T=0$  K. (d)–(f) The corresponding quantities at  $T=300$  K.

uncertainties of the excited state wave packet and their product, for three different times stretching over a half period of the second moment dynamics. The uncertainty product is once again practically independent of time, especially at high temperatures. This is in accord with Eq. (44), which shows that the oscillatory term diminishes rapidly with increasing temperatures and the product attains the limit  $\bar{n}_e + (1 - A_{1e}^2)/2$ .

It is interesting to note from Eq. (40) for  $\bar{n}_e$  that, if we neglect the vibrational frequency in comparison with the electronic dephasing rate constant  $\Gamma_{eg}$  so that  $\Phi_I(\omega \pm \omega_0) = \Phi_I(\omega)$ , we have, using Eq. (33),  $\bar{n}_e \cong \bar{n} + \Delta^2/2$ . This is precisely the mean occupation number for the displaced thermal state as expressed in Eq. (6). We will see in the following that the same limit for  $\bar{n}_e$  is obtained in the ultrashort pulse limit. In contrast, the mean occupation number in the ground state  $\bar{n}_g$  given by Eq. (26) does not attain a simple limit for ultrafast electronic dephasing.

The simulations of the present section serve to illustrate the application of simple yet rigorous expressions for the second moments and their connection to the equilibrium line shapes. It is clear that the detailed behavior of the position and momentum uncertainties can also be evaluated over a wider range of pulse widths and temperature.

### C. Dependence on pulse width

A key ingredient for the creation of nonstationary vibrational states is an ultrashort laser pulse with a bandwidth sufficiently large to excite several vibrational levels. The superposition of many such levels results in a localized wave packet. Since several time scales are involved in the problem, we first define some useful limits. The impulsive limit is when the pulse duration is much shorter than the vibrational period, i.e.,  $\tau_p \ll \omega_0^{-1}$ , with the electronic dephasing time scale remaining arbitrary. If, in addition, the electronic dephasing is much more rapid than the pulse, i.e.,  $\Gamma_{eg}^{-1} \ll \tau_p \ll \omega_0^{-1}$ , we obtain the ‘‘snapshot limit.’’<sup>26</sup> While the condition  $\Gamma_{eg}^{-1} \ll \tau_p$  is justified for many condensed phase systems with broad and featureless absorption spectra, the simulations in Fig. 6 show that the impulsive limit is not generally applicable for all modes in a multimode system with vibrational frequencies spanning the bandwidth of the pump pulse. A more extreme ultrashort pulse limit is defined as that when the pulse duration is shorter than both electronic and vibrational time scales, i.e.,  $\tau_p \ll \Gamma_{eg}^{-1} \ll \omega_0^{-1}$ . This is an interesting limit to consider from a theoretical point of view.

It has generally been recognized that coherent vibrational motion in the ground state vanishes both in the ultrashort pulse limit and in the very long pulse limit.<sup>25,40,52,65</sup> It is obvious that a very long pulse does not have the sufficient bandwidth to excite coherent motion. The vanishing of the ground state coherence in the opposite limit of very short pulses arises due to the fact that the broad spectrum of the laser pulse bleaches all the nuclear coordinates to an equal extent. Thus, a moving hole cannot be induced in the ground state.<sup>40</sup> Both these limits are clearly obtained from the ground state first moments in Eqs. (20a) and (20b) and the second moment amplitude in Eq. (27). For an infinitely long pulse, the pulse envelope spectrum  $\tilde{G}(\omega - \omega_c)$  approaches a delta function and the product spectral function  $\tilde{G}_p(\omega - \omega_c, n\omega_0)$  in the moment expressions is vanishingly small. In the ultrashort pulse limit, we may set  $\tilde{G}_p(\omega - \omega_c, n\omega_0) \cong \tilde{G}^2(\omega - \omega_c)$  and remove it outside the integrals in Eqs. (20a), (20b) and Eq. (27), since  $\tilde{G}^2(\omega - \omega_c)$  varies much more slowly than the line shape functions. The expressions then reduce to integrals over the differences of bounded functions  $\Phi_I(\omega)$  and  $\Phi_R(\omega)$  and hence vanish. It should be noted this occurs only in the ultrashort pulse limit; in the less stringent impulsive limit, the moments are given by Eqs. (B2a) and (B2b).

Turning to the pulse width dependence of the excited state moments, we note that  $\bar{Q}'_e(0)$  also vanishes for long pulses because the product spectral function  $\tilde{G}_p(\omega - \omega_c, \omega_0)$  in Eq. (36a) is negligible. However, the integral in Eq. (36a) does not vanish when the pulse is very short. If we neglect the variation of the pulse spectrum over the absorption line shape, the second term of Eq. (36a) is simply an integral over the derivative of the bounded function  $\Phi_I(\omega)$  and therefore vanishes. We are then left with the first term, which reduces to the following result if we let  $\tilde{G}_p(\omega - \omega_c, \omega_0) \cong \tilde{G}^2(\omega - \omega_c)$  and use Eq. (33):

$$\overline{Q_e'}(t) = -\Delta \cos(\omega_0 t) \quad (\tau_p \rightarrow 0). \quad (47)$$

By making similar approximations in Eqs. (40) and (41), we obtain the following expressions for mean occupation number  $\overline{n_e}$  and the second moment  $\overline{Q_e^2}(t)$  in the ultrashort pulse limit:

$$\overline{n_e} = \overline{n} + \Delta^2/2, \quad (48a)$$

$$\overline{Q_e^2}(t) = \overline{n} + 1/2 + \Delta^2 \cos^2(\omega_0 t). \quad (48b)$$

The moments of  $P(t)$  are simply obtained by substituting  $t \rightarrow t + \pi/2\omega_0$  in Eqs. (48a) and (48b). The position and momentum uncertainties become time independent in the ultrashort pulse limit and approach their thermal equilibrium values given by Eq. (23):

$$\sigma_{Q_e}(t) = \sigma_{P_e}(t) = \sqrt{(\overline{n} + 1/2)}. \quad (49)$$

From Eqs. (47) and (37), we have  $\overline{Q_e}(0) = 0$ . The centroid of the excited state nuclear wave packet is thus initially located vertically above the ground state equilibrium position and oscillates with an amplitude  $\Delta$ . Equations (47)–(49) together imply that for infinitely short pulses, the excited state wave packet is simply the thermal state  $\hat{\rho}_T$ , initially displaced from equilibrium as in Eq. (6) with a coherent displacement  $\lambda_e = \Delta/\sqrt{2}$ . Note that  $|\lambda_e|^2 = \Delta^2/2 = S$  is the quantity usually called the electron nuclear coupling strength, and represents the mean number of phonons in a coherent state that has been displaced by  $\lambda_e$  from the vacuum ( $\overline{n} = 0$ ).

Since the pulse induced ground state coherence vanishes both in the limit of pulses that are too long and too short compared to vibrational and electronic dephasing time scales, we would expect the amplitude of the ground state coherent motion to peak at some intermediate value of the pulse width. We have also seen that the amplitude and phase of the induced vibrational motion is strongly sensitive to the detuning of the laser frequency from the absorption maximum. It is therefore important to consider both the laser pulse width and the carrier frequency if, for instance, one is interested in determining the conditions for generating optimal displacements in the ground state.<sup>36–38</sup> The expressions derived here for the ground and excited state moments are amenable to fast numerical computation. The computational advantage offered by the analytic expressions enables multi-dimensional plots that capture the behavior of the nonequilibrium moments over an entire manifold of pulse widths and carrier frequencies simultaneously. Furthermore, the expressions derived here allow us to incorporate the experimentally measured absorption line shape (and its Kramers–Kronig transform, the dispersion line shape). This enables absolute scale calculations of the pulse induced moments for any given mode in a complex multimode system.

As an example, we consider the heme protein myoglobin (Mb), which is an oxygen storage protein found in muscle cells. Mb possesses a highly asymmetric and broad absorption spectrum (Soret band) in its ligand-free, high spin (deoxy,  $S=2$ ) state. In previous studies, the Soret band of Mb was modeled using a non-Gaussian inhomogeneous distribution<sup>63</sup> of electronic energy levels, ascribed to disorder

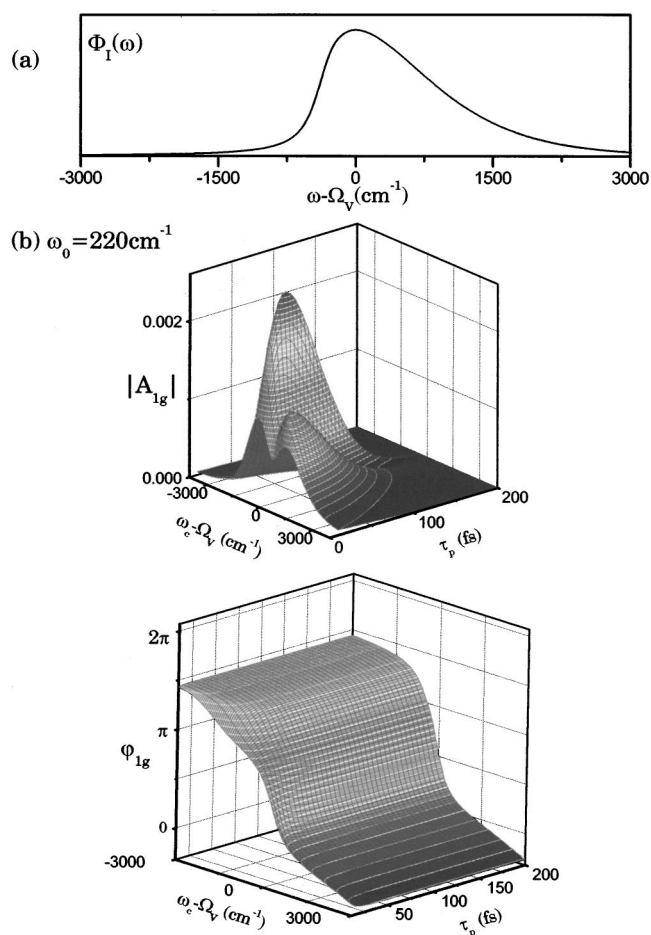


FIG. 9. (a) Absorption line shape for an asymmetric inhomogeneously broadened system, with parameters chosen to mimic the deoxyMb absorption spectrum at room temperature. (b) Three-dimensional view depicting the laser pulse width and carrier frequency dependence of the first moment amplitude  $|A_{1g}|$  and phase  $\varphi_{1g}$ , for the  $220 \text{ cm}^{-1}$  mode (coupling strength  $S=0.05$ ) in the ground electronic state.

in the position of the central iron atom of the porphyrin ring.<sup>69,70</sup> In Fig. 9(a), we plot the simulated absorption line shape with mode coupling strengths and frequencies obtained from previous resonance Raman studies of the Mb Soret line shape.<sup>69,71</sup> Of the numerous modes coupled to the Soret transition, we consider two modes at  $50$  and  $220 \text{ cm}^{-1}$  and study the pump induced initial amplitude and phase for these modes. In Fig. 9(b), we plot the amplitude and phase for the  $220 \text{ cm}^{-1}$  mode in the ground electronic state, as a function of carrier frequency  $\omega_c$  and pulse width  $\tau_p$ . The approach of the ground state amplitude to zero in both the short and long pulse limits is clear from Fig. 9. It is also seen that the laser pulse width for which  $|A_{1g}|$  is maximum is sensitive to the detuning of the pulse center frequency from  $\Omega_v$ . The initial amplitude for excitation on the red side of the absorption maximum is much larger than for excitation toward the blue side of the absorption maximum. This reflects the asymmetry of the Mb absorption spectrum with a much larger slope on the red side than on the blue side of the absorption maximum. Although there are numerous optically coupled modes in the model, the mode specific nature of Eqs. (20a) and (20b) allows us to calculate the nonequilib-

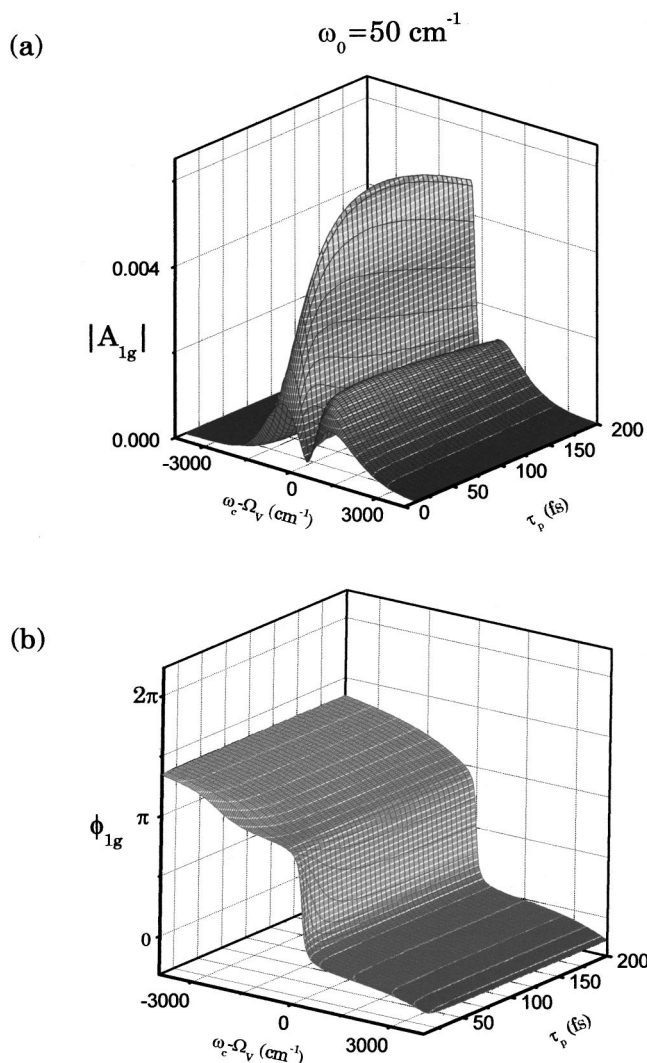


FIG. 10. (a) Three-dimensional plot depicting the laser pulse width and carrier frequency dependence of the pulse induced first moment amplitude profile (a) and phase profile (b) for the 50 cm<sup>-1</sup> mode ( $S=0.1$ ) in the ground state. The mode is coupled to the inhomogeneously broadened system considered in Fig. 9(a).

rium moments for a specific vibrational mode of choice, with the effect of the remaining modes carried through in the equilibrium line shape functions. In Fig. 10, we plot the amplitude and phase of the 50 cm<sup>-1</sup> mode in the ground state. Note that the optimal amplitude of the ground state motion is attained for pulses nearly as long as 100 fs in contrast to the 220 cm<sup>-1</sup> mode which attains an optimal amplitude near 40 fs. The optimal pulse widths are thus not in direct proportion to the vibrational frequencies as one might naively expect.

We plot the initial position of the excited state wave packet  $\bar{Q}_e(0)$  for the 50 and 220 cm<sup>-1</sup> mode in the excited state in Fig. 11. The initial position approaches the excited state equilibrium in the limit of long pulses implying that the oscillations vanish. For very short pulses, the limit expressed in Eq. (47) is clearly obtained, with the position increment approaching zero. As discussed previously, this corresponds to the fact that the excited state wave packet is placed directly above the ground state equilibrium position and oscillates with an amplitude  $\Delta$ . Also, note that the detuning de-

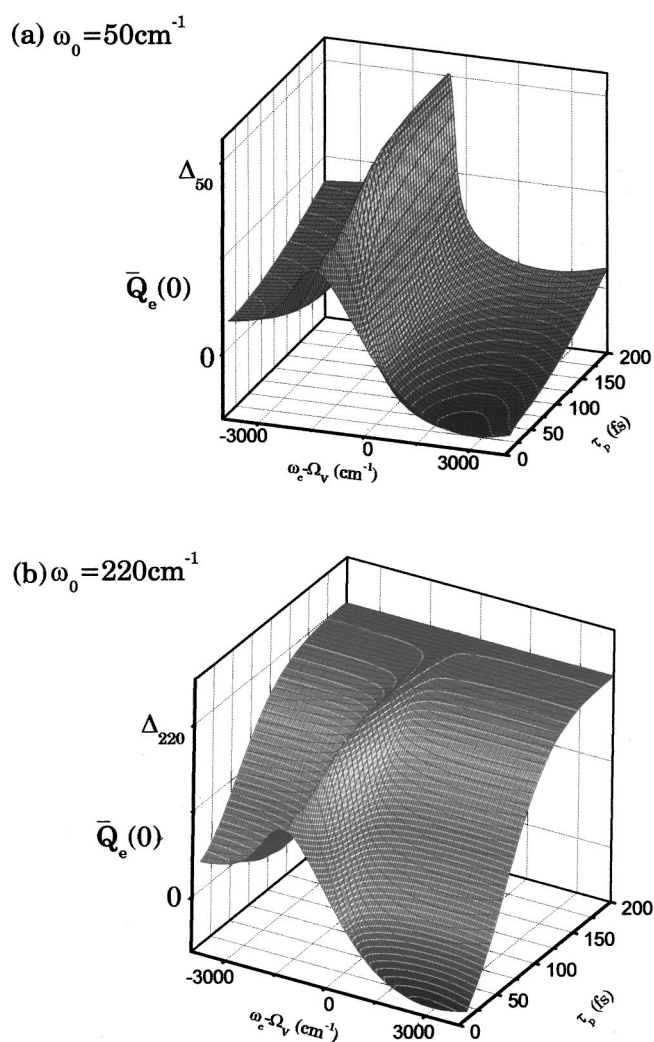


FIG. 11. Dependence of the effective initial position of the excited state wave packet  $\bar{Q}_e(0)$  on laser pulse width and carrier frequency, for the model system considered in Fig. 9(a). (a) The mean position for the 50 cm<sup>-1</sup> mode and (b) the mean position of the 220 cm<sup>-1</sup> mode.

pendence of the excited state position increment is very strongly sensitive to the laser pulse width (see Fig. 5). For very short pulses, the mean position changes its sign with respect to the ground state equilibrium as  $\omega_c$  is tuned across  $\Omega_v$ . As the pulse width becomes longer, the profile of the first moment slowly drifts toward the excited state equilibrium and stays on one side of the ground state equilibrium position for long enough pulses. The three-dimensional simulations presented in Figs. 9–11 capture the highly detailed behavior of the pump induced first moments in position and momentum as a function of pulse width and carrier frequency. The simple analytical formulas presented in this work thus enable us to make fully quantum mechanical quantitative predictions for the laser pulse induced nonstationary vibrational states in complex multimode systems.

## VI. SUMMARY AND CONCLUSIONS

In this paper, we have presented a rigorous analysis of the nonstationary vibrational states prepared by a short laser pulse interacting with a two electronic level system with lin-

ear electron-nuclear coupling. The chief motivation behind this work is to expose the nature of the pump-induced doorway state, using a rigorous moment analysis. A knowledge of the moments of the doorway state provides a convenient starting point for the analysis of pump-probe signals.<sup>27</sup> In the present work, we have used moment generating functions to derive general expressions for arbitrary moments of  $\hat{Q}$  and  $\hat{P}$  in the ground and excited state density matrices to second order in the pump fields.

The fully quantum mechanical expressions for the first two moments of position and momentum reveal interesting behavior with respect to temperature, pump pulse carrier frequency, and width. The pump pulse induced changes of the mean position and momentum in the ground state are found to depend on the derivatives of the absorptive and dispersive line shapes, respectively. This relationship enables one to readily obtain a qualitative understanding of the dependence of pump induced first moment changes on the carrier frequency. The mean position of pump induced ground state exhibits a much stronger temperature dependence than the mean momentum. This implies a strong temperature dependence of the initial phase of the ground state wave packet, and consequently the phase of the pump-probe signal is also strongly temperature dependent.<sup>27</sup> While the ground state moments depend on both the absorptive and dispersive parts of the equilibrium line shape functions, the moments of the excited state wave packet are shown to depend only on the absorptive line shape function. This is strongly indicative of the distinct mechanisms that induce ground and excited state coherences; namely stimulated Raman-type processes for the ground state, and absorptive processes for the excited state. The amplitude of the ground state oscillations decreases uniformly with temperature for all pump carrier frequencies. In contrast, the profile of the excited state first moment amplitude exhibits a striking asymmetry with change in temperature: For red excitation, the amplitude of the excited state wave packet decreases with increased temperature, whereas for blue excitation, the amplitude increases with temperature. This contrasting behavior can be explained based on the particle- versus hole-like nature of the ground and excited state wave packets. It can also be used to experimentally discriminate between the ground and excited state coherences.

An analysis of the second moments of the pump-induced doorway state reveals information regarding the squeezing of the ground and excited state nuclear distributions by the laser pulse interaction. It is well known that a difference in the curvature of the ground and excited state vibrational potentials (quadratic coupling) can induce squeezed vibrational states.<sup>57-60</sup> Apart from this "geometric" squeezing,<sup>57</sup> the laser pulse can by itself induce a time-dependent variance in the vibrational distributions, which is also called "dynamic squeezing."<sup>57</sup> The present analysis exposes the nature of the dynamical squeezing and its relation to the equilibrium absorption and dispersion line shapes. While the first moment dynamics constitutes a major part of the wave-packet motion detected by the probe,<sup>27</sup> higher moment modulations, such as squeezing, will contribute weakly to overtone signals. We have recently presented an analysis of the overtone signals

generated due to purely geometric squeezing in the context of nonradiative reactions.<sup>27</sup> The analysis of overtone signals generated by dynamical squeezing due to the laser pulse interaction will be the subject of future work.

We have pointed out the consequence of the second-order perturbative approximation to the doorway density matrix. Since a genuine change in the ground state vibrational populations requires a fourth-order interaction (stimulated Raman scattering) of the pump pulse, the diagonal density matrix elements calculated using only the second-order approximation will be inaccurate. The neglect of higher order field interactions results in certain discrepancies in the calculated expectation values of the higher moments. For example, we showed that the ground state doorway (to second order) violates the properties of a genuine density matrix, and leads to a position-momentum uncertainty product that is in violation of the uncertainty principle. While these aspects have been noted in earlier work,<sup>37,40</sup> we have presented an estimate of the error due to truncation at second order.

Perhaps the most important aspect of the present analysis is the direct connection made between the laser pulse induced nonstationary states and the measurable equilibrium properties of the system. This connection appears through the dependence of the pump-induced moments on the equilibrium line shape functions. A direct consequence of this aspect is that the pump induced moments are highly mode specific; the only explicit parameters in the moment expressions are the mode frequency and coupling strength. The rest of the parameters relevant to the system and the bath are automatically carried by the measured line shape functions. One practical consequence is a many-fold increase in computational efficiency. In this respect, the present approach must be contrasted with earlier treatments that expressed the full second-order doorway density matrix using the more cumbersome sum over vibronic eigenstates expressions.<sup>29,50</sup> Here we have shown that the individual moments of the doorway density matrix can be calculated efficiently using a correlation function based approach.

Apart from computational advantages, the direct connection with equilibrium line shape functions can potentially be exploited in calculating the various moments on an absolute (per molecule) scale. Since absolute scale measurements of the absorption cross section are possible experimentally, one may use the Kramers-Kronig relations to calculate the dispersion line shape, and subsequently incorporate the line shapes in the moment expressions. This would yield precise values for moments of the nonstationary wave packet induced by the pump pulse for any given mode in a complex multimode system. This approach is analogous to transform methods previously used to describe resonance Raman scattering.<sup>42-46,72</sup>

We finally mention that the present work can be extended beyond the linearly coupled harmonic oscillator model assumed here. Quadratic electron-nuclear coupling can be treated using standard quantum field theoretic techniques. Non-Condon effects can also be readily incorporated by assuming an exponential dependence of the dipole moment on the nuclear coordinate.<sup>52,73</sup> Furthermore, a calculation of the moments for multiple pulse excitation<sup>36-38</sup> can

also be carried out along the same lines as the calculation presented here. The central point is that the initial state (before the pulse interactions) is a thermal density matrix. The multitime correlation functions can therefore be evaluated exactly using a second-order cumulant expansion.

A moment analysis of the doorway state can also be envisaged in spectroscopies that use multiply resonant pulses with different carrier frequencies. For instance, consider a time domain coherent anti-Stokes Raman spectroscopy experiment<sup>26,74</sup> involving two time coincident pulses with wave vectors  $\mathbf{k}_1$  and  $\mathbf{k}_2$ , which are followed by delayed pulse with wave vector  $\mathbf{k}_1$ . The measured signal is the total coherent emission along the direction  $\mathbf{k}_s = 2\mathbf{k}_1 - \mathbf{k}_2$ . In this case, the relevant term in the third-order polarization consists of contributions from three fields, one from each of the three pulses.<sup>26</sup> The first two fields (from the time coincident pulses) prepare a second-order doorway state. The corresponding density matrix can be calculated by replacing the two pump fields  $E_a(t)$  in the second-order expression for the doorway density matrix [given in Eq. (3)] by the fields from the two different pulses. One would then evaluate the various moments for this density matrix, and subsequently make a displaced thermal state representation as in Eq. (6). The third-order polarization induced by the delayed pulse may then be calculated using the effective linear response approach.<sup>27</sup> A rigorous analysis of these experiments requires the inclusion of the spatial dependence of the laser fields and will be considered in future work.

## APPENDIX A: MOMENTS OF NUCLEAR POSITION AND MOMENTUM IN THE DOORWAY STATE

### 1. Ground state

The moment generating function for the coordinate  $\hat{Q}(t)$ , for the density matrix  $\hat{\rho}_g$  is defined as

$$\mathcal{M}_Q^{(g)}(k, t) = (1/\mathcal{N}_g) \text{Tr}[e^{ik\hat{Q}(t)} \hat{\rho}_g], \quad (\text{A1})$$

where  $\mathcal{N}_g$  is given by Eq. (15). The time evolution of  $\hat{Q}$  in Eq. (A1) is governed by the ground state Hamiltonian  $\hat{H}_g$  and takes the following form for  $\hat{H}_g$  defined in Eq. (10a):

$$\hat{Q}(t) = \hat{Q} \cos(\omega_0 t) + \hat{P} \sin(\omega_0 t). \quad (\text{A2})$$

From a knowledge of  $\mathcal{M}_Q^{(g)}(k, t)$ , we can calculate the time-dependent moments of  $\hat{Q}$  for the pump induced density matrix by a simple differentiation of  $\mathcal{M}_Q^{(g)}(k, t)$ :

$$\overline{Q_g^n}(t) = (-i)^n (\partial^n \mathcal{M}_Q^{(g)}(k, t) / \partial k^n)_{k=0}. \quad (\text{A3})$$

Also, since it follows from Eq. (A1) and the definition in Eq. (5) that

$$\mathcal{M}_Q^{(g)}(k, t) = \sum_{n=0}^{\infty} \frac{(ik)^n}{n!} \overline{Q_g^n}(t), \quad (\text{A4})$$

the moments can be directly obtained as the coefficients of the various powers of  $k$  in the series expansion for  $\mathcal{M}_Q^{(g)}(k, t)$ . The moments of  $\hat{P}(t)$  are trivially obtained from the coordinate moments by letting  $t \rightarrow t + \pi/2\omega_0$ . To see this, consider the Hamilton's equation  $d\hat{Q}(t)/dt = \omega_0 \hat{P}(t)$  and the

relation  $d\hat{Q}(t)/dt = \omega_0 \hat{Q}(t + \pi/2\omega_0)$  that follows from Eq. (A2). These two equations imply the operator relation  $\hat{P}(t) = \hat{Q}(t + \pi/2\omega_0)$  so that the  $n$ th moments of  $\hat{Q}$  and  $\hat{P}$  obey

$$\overline{P_g^n}(t) = \overline{Q_g^n}(t + \pi/2\omega_0). \quad (\text{A5})$$

We now derive a fully quantum-mechanical expression for  $\mathcal{M}_Q^{(g)}(k, t)$ . Using Eq. (A1) and Eq. (9), we have

$$\begin{aligned} \mathcal{M}_Q^{(g)}(k, t) = & (1/\mathcal{N}_g) \left\langle \left\langle e^{ik\hat{Q}(t)} \right\rangle_T - \frac{|\mu_{ge}|^2}{\hbar^2} \int_{-\infty}^{\infty} dt' \int_0^{\infty} ds \right. \\ & \times E(t') E(t' - s) e^{-\Gamma_{eg}|s|} \\ & \left. \times [e^{-i\Omega_v s} A_k^g(t - t', s) + e^{i\Omega_v s} B_k^g(t - t', s)] \right\rangle, \end{aligned} \quad (\text{A6})$$

where we have defined

$$A_k^g(t - t', s) = \left\langle e^{ik\hat{Q}(t)} \exp\left(i\omega_0 \Delta \int_{t'-s}^{t'} ds' \hat{Q}(s')\right) \right\rangle_+, \quad (\text{A7a})$$

$$B_k^g(t - t', s) = \left\langle \exp\left(-i\omega_0 \Delta \int_{t'-s}^{t'} ds' \hat{Q}(s')\right) e^{ik\hat{Q}(t)} \right\rangle_-. \quad (\text{A7b})$$

The angular brackets  $\langle \rangle_T$  denote the average with respect to the thermal state  $\hat{\rho}_T^{(g)}$  [see Eq. (8)]. The thermal average can be evaluated exactly using a second-order cumulant expansion (which is exact for a thermal state, according to Wick's theorem<sup>75</sup>), with the result

$$\begin{aligned} A_k^g(t - t', s) = & e^{-g(s) + i\omega_0 s \Delta^2/2} e^{-(2\bar{n}+1)k^2/4} \\ & \times \exp\left(-\frac{k\Delta}{2} \mathcal{G}(t - t', s)\right), \end{aligned} \quad (\text{A8a})$$

$$\begin{aligned} B_k^g(t - t', s) = & e^{-g^*(s) - i\omega_0 s \Delta^2/2} e^{-(2\bar{n}+1)k^2/4} \\ & \times \exp\left(\frac{k\Delta}{2} \mathcal{G}^*(t - t', s)\right). \end{aligned} \quad (\text{A8b})$$

Here, we have defined the function  $\mathcal{G}(t, s)$  [which arises from the cross terms that result from the cumulant expansion in Eqs. (A7a) and (A7b)] as

$$\mathcal{G}(t, s) = -i[(\bar{n}+1)e^{-i\omega_0 t}(1 - e^{-i\omega_0 s}) - \bar{n}e^{i\omega_0 t}(1 - e^{i\omega_0 s})], \quad (\text{A9})$$

and  $g(s)$  is given by Eq. (12) for the undamped harmonic oscillator. If we expand  $A_k^g$  and  $B_k^g$  in powers of  $k$  and substitute the resulting expression into Eq. (A6), and compare the result with Eq. (A4), we get

$$\begin{aligned} \overline{Q_g^n}(t) = & \sum_{l=0}^{\infty} \delta_{n,2l} \frac{n!(2\bar{n}+1)^l}{2^n \mathcal{N}_g} + \frac{n!}{(2i)^n \mathcal{N}_g} \sum_{l=0}^{\infty} \sum_{m=0}^{\infty} \delta_{n,2l+m} \\ & \times \frac{(-1)^{l+m}}{l!m!} \Delta^m (2\bar{n}+1)^l [\mathcal{C}_m(t) + (-1)^m \mathcal{C}_m^*(t)], \end{aligned} \quad (\text{A10})$$

with

$$C_m(t) = -\frac{|\mu_{ge}|^2}{\hbar^2} \int_{-\infty}^{\infty} dt' \int_0^{\infty} ds E(t') E(t'-s) \times e^{-\Gamma_{eg}|s| - i\Omega_{00}s - g(s)} [\mathcal{G}(t-t', s)]^m. \quad (\text{A11})$$

Here,  $\delta_{i,j}$  refers to the Kronecker's delta. The first term in Eq. (A10) gives the moments of the equilibrium state  $\hat{\rho}_T^{(g)}$ . Equations (A10) and (A11) along with Eqs. (A9) and (12) provide the complete set of expressions required to calculate arbitrary moments of the coordinate operator in the pump induced density matrix. The moments of  $\hat{P}(t)$  are obtained using Eq. (A5).

## 2. Excited state

Consider the coordinate operator  $\hat{Q}$  evolving in time due to  $\hat{H}_e$  defined in Eq. (10b):

$$\hat{Q}_e(t) = \Delta + (\hat{Q} - \Delta) \cos(\omega_0 t) + \hat{P} \sin(\omega_0 t). \quad (\text{A12})$$

This has the expected form, with the constant  $\Delta$  reflecting the oscillations about the excited state equilibrium position. In evaluating the excited state moments, it is more convenient to shift the origin to  $\Delta$  and take  $\hat{Q}'_e(t) = \hat{Q}_e(t) - \Delta$  for the excited state oscillator coordinate. The creation (destruction) operators for the excited state oscillator with a shifted equilibrium position are defined as

$$\hat{Q} - \Delta = (\hat{a}_e + \hat{a}_e^\dagger) / \sqrt{2}; \hat{P} = i(\hat{a}_e^\dagger - \hat{a}_e) / \sqrt{2}. \quad (\text{A13})$$

From Eq. (10b), the excited state Hamiltonian is given as  $\hat{H}_e = \hbar\omega_0(\hat{a}_e^\dagger \hat{a}_e + 1/2) - \hbar\omega_0\Delta^2/2$ . The moment generating function is then defined analogous to Eq. (A1) but with the substitution  $\hat{Q}(t) \rightarrow \hat{Q}'_e(t)$  and  $g \rightarrow e$ :

$$\mathcal{M}_{\hat{Q}}^{(e)}(k, t) = (1/\mathcal{N}_e) \text{Tr}[e^{ik\hat{Q}'_e(t)} \hat{\rho}_e], \quad (\text{A14})$$

where  $\mathcal{N}_e$  is the excited state population given by Eq. (33). Using Eq. (A2), we also have  $\hat{Q}'_e(t) = \hat{Q}(t) - \Delta \cos(\omega_0 t)$  so that

$$\mathcal{M}_{\hat{Q}}^{(e)}(k, t) = (1/\mathcal{N}_e) \text{Tr}[e^{ik\hat{Q}(t)} \hat{\rho}_e] e^{-ik\Delta \cos(\omega_0 t)}. \quad (\text{A15})$$

Analogous to Eq. (A5), the moments of the  $\hat{P}$  for the excited state can be obtained from the coordinate moments by the substitution  $t \rightarrow t + \pi/2\omega_0$ . For the coordinate moments, we have from Eqs. (32) and (A14)

$$\mathcal{M}_{\hat{Q}}^{(e)}(k, t) = \frac{|\mu_{ge}|^2}{\mathcal{N}_e \hbar^2} \int_{-\infty}^{\infty} dt' \int_{-\infty}^{t'} dt'' E(t') E(t'') e^{-\Gamma_{eg}|s|} \times [e^{i\Omega_{0v}s} A_k^e(t, t', t'') + e^{-i\Omega_{0v}s} A_k^e(t, t'', t')], \quad (\text{A16})$$

where  $s = t' - t''$  and we have defined

$$A_k^e(t, t', t'') = \exp(-ik\Delta \cos(\omega_0 t)) \times \left\langle \left( \exp\left( i\omega_0 \Delta \int_0^{t''} ds' \hat{Q}(s') \right) \right)_+ \times \exp(ik\hat{Q}(t)) \left( \exp\left( -i\omega_0 \Delta \int_0^{t'} ds' \hat{Q}(s') \right) \right)_- \right\rangle_T. \quad (\text{A17})$$

The thermal average in Eq. (A17) can be evaluated similar to Eqs. (A7a) and (A7b), using a second-order cumulant expansion. We find

$$A_k^e(t, t', t'') = e^{-g^*(s) - i\omega_0 s \Delta^2/2} e^{-(2\bar{n}+1)k^2/4} \times \exp\left( -\frac{k\Delta}{2} \mathcal{G}_e(t, t', t'') \right), \quad (\text{A18})$$

where  $g(s)$  is defined in Eq. (12), and

$$\mathcal{G}_e(t, t', t'') = i[e^{-i\omega_0 t}((\bar{n}+1)e^{i\omega_0 t'} - \bar{n}e^{i\omega_0 t''}) + e^{i\omega_0 t}((\bar{n}+1)e^{-i\omega_0 t''} - \bar{n}e^{-i\omega_0 t'})]. \quad (\text{A19})$$

[Note that  $\mathcal{G}_e(t, t'', t') = -\mathcal{G}_e^*(t, t', t'')$ .] Expansion of  $A_k$  in powers of  $k$  and substituting the result in Eq. (A16) gives us the final result:

$$\mathcal{M}_{\hat{Q}}^{(e)}(k, t) = \sum_{n=0}^{\infty} \frac{(ik)^n}{n!} \overline{Q}_e^{(n)}(t), \quad (\text{A20})$$

where

$$\overline{Q}_e^{(n)}(t) = \frac{n!}{(2i)^n \mathcal{N}_e} \sum_{l=0}^{\infty} \sum_{m=0}^{\infty} \delta_{n, 2l+m} \frac{(-1)^{l+m}}{l!m!} \Delta^m (2\bar{n}+1)^l \times [\mathcal{D}_m(t) + (-1)^m \mathcal{D}_m^*(t)], \quad (\text{A21})$$

with

$$\mathcal{D}_m(t) = \frac{|\mu_{ge}|^2}{\hbar^2} \int_{-\infty}^{\infty} dt' \int_{-\infty}^{t'} dt'' E(t') E(t'') \times e^{-\Gamma_{eg}|s| + i\Omega_{00}s - g^*(s)} [\mathcal{G}_e(t, t', t'')]^m. \quad (\text{A22})$$

Equations (A21) and (A22) along with Eqs. (A19) and (12) provide the complete set of expressions required to calculate arbitrary moments of the coordinate operator for the pump induced excited state density matrix. Extension of the main results in this section to the multimode harmonic case and for damped oscillators is straightforward, but is not considered here for simplicity.

## APPENDIX B: COHERENT MOTION IN THE IMPULSIVE LIMIT

Here we consider the impulsive limit of the first moment results obtained in Secs. III B and IV B, by assuming that the laser pulse duration is much shorter than the vibrational period. Consider the ground state first moments in Eqs. (20a)

and (20b). Before we make the short pulse approximation, we rewrite the two equations after making a simple change of variables:

$$\bar{Q}_g(0) = -\frac{|\mu_{ge}|^2 E_0^2 (2\bar{n}+1)\Delta}{8\pi\hbar^2 \mathcal{N}_g} \int_0^\infty d\omega \Phi_I(\omega) \tilde{G}(\omega - \omega_c) \times [\tilde{G}(\omega - \omega_c - \omega_0) - \tilde{G}(\omega - \omega_c + \omega_0)], \quad (\text{B1a})$$

$$\bar{P}_g(0) = \frac{|\mu_{ge}|^2 E_0^2 \Delta}{8\pi\hbar^2 \mathcal{N}_g} \int_0^\infty d\omega \Phi_R(\omega) \tilde{G}(\omega - \omega_c) \times [\tilde{G}(\omega - \omega_c - \omega_0) - \tilde{G}(\omega - \omega_c + \omega_0)]. \quad (\text{B1b})$$

If we now make the approximation,  $\tau_p^{-1} \gg \omega_0$ , we may replace the expressions within square brackets in Eqs. (B1a) and (B1b) by the first derivatives of the pulse spectrum. A subsequent integration by parts then leads to final results,

$$\bar{Q}_g^{(\text{Imp})}(0) = -\frac{|\mu_{ge}|^2 E_0^2 (2\bar{n}+1)\omega_0 \Delta}{8\pi\hbar^2 \mathcal{N}_g} \times \int_0^\infty d\omega \tilde{G}^2(\omega - \omega_c) (\partial\Phi_I(\omega)/\partial\omega), \quad (\text{B2a})$$

$$\bar{P}_g^{(\text{Imp})}(0) = \frac{|\mu_{ge}|^2 E_0^2 \omega_0 \Delta}{8\pi\hbar^2 \mathcal{N}_g} \times \int_0^\infty d\omega \tilde{G}^2(\omega - \omega_c) (\partial\Phi_R(\omega)/\partial\omega). \quad (\text{B2b})$$

The only assumption made in deriving the above results is that the pulse duration is short compared to the vibrational period. The temperature, (linear) electron-nuclear coupling strength, and all other line shape parameters remain arbitrary. It is seen that in the impulsive limit, the position and momentum increments are simply given by the convolution of the laser pulse spectrum with the derivatives of the absorption and dispersion line shapes, respectively. Also, the effect of the spectral bandwidth of the laser pulse enters the above expressions independently of the mode frequency, in contrast to the general expressions (20a) and (20b).

The impulsive limit of the excited state coherence can be similarly obtained from Eq. (36a). We find,

$$\bar{Q}_e^{(\text{Imp})}(0) = -\frac{|\mu_{ge}|^2 E_0^2 \Delta}{4\pi\hbar^2 \mathcal{N}_e} \int_0^\infty d\omega \tilde{G}^2(\omega - \omega_c) \times [\Phi_I(\omega) - \bar{n}\omega_0 (\partial\Phi_I(\omega)/\partial\omega)]. \quad (\text{B3})$$

A closed form solution is possible for the mean position if we approximate the imaginary part of the line shape to be Gaussian, which is realized in the semiclassical limit of high temperatures or strong electron-nuclear coupling strengths.<sup>76</sup> As an illustration, we obtain a closed form expression for the ground state by taking the following forms for the Gaussian spectral function and the imaginary part of the line shape function:

$$\tilde{E}(\omega) = \frac{E_0}{2} (2\pi\tau_p^2)^{1/2} e^{-(\omega - \omega_c)^2 \tau_p^2 / 2}, \quad (\text{B4})$$

$$\Phi_I(\omega) = \sqrt{\pi/2\sigma_T^2} e^{-(\omega - \Omega_v)^2 / 2\sigma_T^2}, \quad (\text{B5})$$

where the semiclassical linewidth is given by  $\sigma_T = \Delta \sqrt{k_B T \omega_0 / \hbar}$ . Using these definitions in Eq. (B2a), we get

$$\bar{Q}_g^{(\text{Imp})}(0) = \frac{(2\pi)^{3/2} \omega_0 |\mu_{ge}|^2 E_0^2 \tau_p^2 \Delta (2\bar{n}+1)}{16\pi\hbar^2 \sigma_T^3} \times \int_0^\infty d\omega (\omega - \Omega_v) \times e^{-(\omega - \omega_c)^2 \tau_p^2 - (\omega - \Omega_v)^2 / 2\sigma_T^2}. \quad (\text{B6})$$

Evaluation of the above-mentioned integral gives the final result,

$$\bar{Q}_g^{(\text{Imp})}(0) = \frac{C \omega_0 \tau_p^4 \Delta (\omega_c - \Omega_v) (2\bar{n}+1)}{(1 + 2\tau_p^2 \sigma_T^2)^{3/2}} \times \exp\left[-\frac{\tau_p^2}{(1 + 2\tau_p^2 \sigma_T^2)} (\omega_c - \Omega_v)^2\right], \quad (\text{B7})$$

where we have defined the constant  $C = \pi |\mu_{ge}|^2 E_0^2 / 2\hbar^2$ . Equation (B7), valid in the impulsive limit of short pulses, captures several of the features found from the general result in Eq. (20a). The initial amplitude is seen to change its phase across the absorption maximum  $\Omega_v$ . The sign of the displacement is opposite to that of the excited state equilibrium shift  $\Delta$  for red detuning from the absorption maximum, while it has the same sign for blue detuning. The ground state displacement vanishes for very short pulses. If, in addition to the impulsive limit where  $\omega_0 \ll \tau_p^{-1}$ , the condition  $\sigma_T \gg \tau_p^{-1}$  is also satisfied (yielding the snapshot limit<sup>26</sup>), Eq. (B7) reduces to

$$\bar{Q}_g^{(\text{Imp})}(0) = \frac{C \omega_0 \tau_p \Delta (\omega_c - \Omega_v) (2\bar{n}+1)}{\sqrt{8}\sigma_T^3} \times \exp[-(\omega_c - \Omega_v)^2 / 2\sigma_T^2], \quad (\text{B8})$$

so that the mean position has a linear dependence on the pulse width.

<sup>1</sup>M. J. Rosker, F. W. Wise, and C. L. Tang, Phys. Rev. Lett. **57**, 321 (1986).

<sup>2</sup>S. Ruhman, A. G. Joly, and K. A. Nelson, J. Chem. Phys. **86**, 6563 (1987).

<sup>3</sup>Y. Yan and K. Nelson, J. Chem. Phys. **87**, 6257 (1987).

<sup>4</sup>Y. Yan and K. A. Nelson, J. Chem. Phys. **87**, 6240 (1987).

<sup>5</sup>Y. X. Yan, L. T. Cheng, and K. A. Nelson, in *Advances in Non-linear Spectroscopy*, edited by R. J. H. Clark and E. Hester (Wiley, Chichester, 1988), p. 299.

<sup>6</sup>A. M. Walsh and R. F. Loring, Chem. Phys. Lett. **160**, 299 (1989).

<sup>7</sup>A. H. Zewail, Science **242**, 1645 (1988).

<sup>8</sup>H. L. Fragnito, J. Y. Bigot, P. C. Becker, and C. V. Shank, Chem. Phys. Lett. **160**, 101 (1989).

<sup>9</sup>N. F. Scherer, R. J. Carlson, A. Matro, M. Du, A. J. Ruggeiro, V. R. Rochin, J. A. Cina, G. R. Fleming, and S. A. Rice, J. Chem. Phys. **95**, 1487 (1991).

<sup>10</sup>W. T. Pollard and R. A. Mathies, Annu. Rev. Phys. Chem. **43**, 497 (1992).

<sup>11</sup>S. L. Dexheimer, Q. Wang, L. A. Peteanu, W. T. Pollard, R. A. Mathies, and C. V. Shank, Chem. Phys. Lett. **188**, 61 (1992).

<sup>12</sup>A. Zewail, J. Phys. Chem. **97**, 12427 (1993).

- <sup>13</sup>M. H. Vos, F. Rappaport, J. C. Lambry, J. Breton, and J. L. Martin, *Nature* (London) **363**, 320 (1993).
- <sup>14</sup>T. P. Dougherty, G. P. Weiderrecht, K. A. Nelson, M. H. Garret, H. P. Jensen, and C. Warde, *Science* **258**, 770 (1992).
- <sup>15</sup>L. Dhar, J. A. Rogers, and K. A. Nelson, *Chem. Rev.* **94**, 157 (1994).
- <sup>16</sup>L. Zhu, J. T. Sage, and P. M. Champion, *Science* **266**, 629 (1994).
- <sup>17</sup>Q. Wang, R. W. Schoenlein, L. A. Peteanu, R. A. Mathies, and C. V. Shank, *Science* **266**, 422 (1994).
- <sup>18</sup>S. E. Bradforth, T. Jiminez, F. V. Mourik, R. V. Grondelle, and G. R. Fleming, *J. Phys. Chem.* **99**, 16179 (1995).
- <sup>19</sup>D. M. Jonas, M. J. Lang, Y. Nagasawa, T. Joo, and G. R. Fleming, *J. Phys. Chem.* **100**, 12660 (1996).
- <sup>20</sup>M. Chachisvilis and V. Sundstrom, *J. Chem. Phys.* **104**, 5734 (1996).
- <sup>21</sup>M. Chachisvilis and V. Sundstrom, *Chem. Phys. Lett.* **234**, 141 (1995).
- <sup>22</sup>T. S. Yang, M. S. Chang, M. Hayashi, S. H. Lin, P. Vohringer, W. Dietz, and N. F. Scherer, *J. Chem. Phys.* **110**, 12070 (1999).
- <sup>23</sup>R. W. Hellwarth, *Prog. Quantum Electron.* **5**, 1 (1977).
- <sup>24</sup>S. Mukamel, *Phys. Rep.* **93**, 1 (1982).
- <sup>25</sup>W. T. Pollard, S. L. Dexheimer, Q. Wang, L. A. Peteanu, C. V. Shank, and R. A. Mathies, *J. Phys. Chem.* **96**, 6147 (1992).
- <sup>26</sup>S. Mukamel, *Principles of Nonlinear Optical Spectroscopy* (Oxford University Press, New York, 1995).
- <sup>27</sup>A. T. N. Kumar, F. Rosca, A. Widom, and P. M. Champion, *J. Chem. Phys.* **114**, 701 (2001). We note a correction to Eq. (44a) of this reference, which gives the amplitude of the open band pump-probe signal. The correct form of Eq. (44a) is:
- $$A_{sk} = \left| \int_0^{\infty} d\omega \mathcal{C}_k(\omega) \right|,$$
- i.e., the absolute value must be taken after the integration over all frequencies.
- <sup>28</sup>Y. J. Yan, L. E. Fried, and S. Mukamel, *J. Phys. Chem.* **93**, 8149 (1989).
- <sup>29</sup>Y. J. Yan and S. Mukamel, *Phys. Rev. A* **41**, 6485 (1990).
- <sup>30</sup>S. Mukamel, *Annu. Rev. Phys. Chem.* **41**, 647 (1990).
- <sup>31</sup>B. Fain and S. Lin, *Chem. Phys.* **161**, 515 (1992).
- <sup>32</sup>B. Fain, S. Lin, and V. Khidekel, *Phys. Rev. A* **47**, 3222 (1993).
- <sup>33</sup>B. Fain and S. Lin, *Chem. Phys. Lett.* **207**, 287 (1993).
- <sup>34</sup>F. Rosca, A. T. N. Kumar, X. Ye, T. Sjudin, A. A. Demidov, and P. M. Champion, *J. Phys. Chem.* **104**, 4280 (2000).
- <sup>35</sup>R. Kosloff, A. D. Hemmerich, and D. Tannor, *Phys. Rev. Lett.* **69**, 2172 (1992).
- <sup>36</sup>J. A. Cina and T. J. Smith, *J. Chem. Phys.* **98**, 9211 (1993).
- <sup>37</sup>T. J. Smith and J. A. Cina, *J. Chem. Phys.* **104**, 1272 (1996).
- <sup>38</sup>T. J. Smith, L. Ungar, and J. A. Cina, *J. Lumin.* **58**, 66 (1994).
- <sup>39</sup>D. M. Jonas and G. R. Fleming, in *Vibrationally Abrupt Pulses in Pump-probe Spectroscopy*, edited by M. El-Sayed (Blackwell Scientific, Oxford, 1994), p. 225.
- <sup>40</sup>D. M. Jonas, S. Bradforth, S. Passino, and G. Fleming, *J. Phys. Chem.* **99**, 2594 (1995).
- <sup>41</sup>U. Banin, A. Bartana, S. Ruhman, and R. Kosloff, *J. Chem. Phys.* **101**, 8461 (1994).
- <sup>42</sup>V. Hizhnyakov and I. Tehver, *Phys. Status Solidi* **21**, 755 (1967).
- <sup>43</sup>J. Page and D. Tonks, *J. Chem. Phys.* **75**, 5694 (1981).
- <sup>44</sup>B. R. Stallard, P. M. Champion, P. Callis, and A. C. Albrecht, *J. Chem. Phys.* **78**, 712 (1983).
- <sup>45</sup>K. T. Schomacker and P. M. Champion, *J. Chem. Phys.* **90**, 5982 (1989).
- <sup>46</sup>J. B. Page, in *Light Scattering in Solids VI*, edited by M. Cardona and G. Guntherodt (Springer, Berlin, 1991), p. 17.
- <sup>47</sup>Y. R. Shen, *The Principles of Nonlinear Optics* (Wiley, New York, 1984).
- <sup>48</sup>S. Mukamel, *Phys. Rev. A* **28**, 3480 (1983).
- <sup>49</sup>R. W. Boyd and S. Mukamel, *Phys. Rev. A* **29**, 1973 (1984).
- <sup>50</sup>B. Fain and S. Lin, *J. Chem. Phys.* **93**, 6387 (1990).
- <sup>51</sup>L. W. Ungar and J. A. Cina, *Adv. Chem. Phys.* **100**, 171 (1997).
- <sup>52</sup>Y. Tanimura and S. Mukamel, *J. Opt. Soc. Am. B* **10**, 2263 (1993).
- <sup>53</sup>T. J. Dunn, I. A. Walmsley, and S. Mukamel, *Phys. Rev. Lett.* **74**, 884 (1995).
- <sup>54</sup>Once the moments are evaluated in the well-separated limit, the effective initial values of the moments are obtained by extrapolation back to  $t=0$ . This procedure is implicit in Eq. (5), where the density matrix is time independent in the WSP limit, and setting  $t=0$  directly gives the extrapolated initial values.
- <sup>55</sup>The displacement operator is the generator of coherent states of the harmonic oscillator from the vacuum state. Coherent states are the nearest approximation to classical states of the oscillator, and derive their name due to their quantum statistical properties. See, for example, J. R. Klauder and E. C. G. Sudarshan, *Fundamentals of Quantum Optics* (Benjamin, New York, 1968).
- <sup>56</sup>Y. Gu, G. A. Widom, and P. M. Champion, *J. Chem. Phys.* **100**, 2547 (1994).
- <sup>57</sup>J. Janszky, A. Vinogradov, I. Walmsley, and J. Mostowski, *Phys. Rev. A* **50**, 732 (1994).
- <sup>58</sup>O. V. Misochko, K. Kisoda, K. Sakai, and S. Nakashima, *Appl. Phys. Lett.* **76**, 961 (2000).
- <sup>59</sup>O. V. Misochko, *Phys. Lett. B* **269**, 97 (2000).
- <sup>60</sup>O. V. Misochko, K. Sakai, and S. Nakashima, *Phys. Rev. B* **61**, 11225 (2000).
- <sup>61</sup>L. D. Landau and E. M. Lifshitz, *Quantum Mechanics*, 3rd ed. (Pergamon, New York, 1977).
- <sup>62</sup>Y. C. Shen and J. A. Cina, *J. Chem. Phys.* **110**, 9793 (1999).
- <sup>63</sup>We note that in a complete pump-probe calculation using the effective linear response approach, the line shape functions appear in two stages,<sup>27</sup> first, in the pump induced moments, as described in the present work, and second, in the probe detection step. In other words, the pump-probe signal is quadratic in the line shape functions. When incorporating experimentally measured line shapes, inhomogeneities (if present) must first be deconvolved from the line shapes before they are employed in both the pump (moment analysis) and probe steps of the calculation. The final pump-probe signal is obtained by convolving the inhomogeneities into the homogeneous signal (Ref. 27). This procedure is analogous to that employed in the calculation of Raman excitation profiles using complex line shape functions (Ref. 46).
- <sup>64</sup>We note that vibrational damping is neglected only for those modes whose moments are being analyzed. One can still allow for damping in the remaining subspace of the system, which appear solely through the line shape function. Thus, in the example considered in Fig. 1(b), the effect of the overdamped 10 cm<sup>-1</sup> mode on the undamped 50 cm<sup>-1</sup> mode under analysis is manifested solely through the line shape function. For all the modes involved in the line shape function (other than the mode of interest), it is justified to use the rigorous expressions for the correlation function  $g(s)$  derived for the damped oscillator case. When one needs to calculate the *pump induced moments of the damped modes*, however, the undamped expressions for the correlation functions  $\mathcal{G}(t-t',s)$  and  $\mathcal{G}_e(t,t',t'')$  [Eqs. (A9) and (A19)] need to be replaced by the corresponding expressions for the damped oscillator case.
- <sup>65</sup>W. Pollard, S. Lee, and R. Mathies, *J. Chem. Phys.* **92**, 4012 (1990).
- <sup>66</sup>S. L. Dexheimer, A. D. V. Pelt, J. A. Brozik, and B. I. Swanson, *J. Phys. Chem.* **104**, 4308 (2000).
- <sup>67</sup>M. Cho, G. R. Fleming, and S. Mukamel, *J. Chem. Phys.* **98**, 5314 (1992).
- <sup>68</sup>M. Cho, M. Du, N. F. Scherer, G. R. Fleming, and S. Mukamel, *J. Chem. Phys.* **99**, 2410 (1993).
- <sup>69</sup>V. Srajer, K. T. Schomacker, and P. M. Champion, *Phys. Rev. Lett.* **57**, 1267 (1986).
- <sup>70</sup>P. M. Champion, *J. Raman Spectrosc.* **23**, 557 (1992).
- <sup>71</sup>V. Srajer, Ph.D. thesis, Northeastern University, 1991.
- <sup>72</sup>P. M. Champion and A. C. Albrecht, *Annu. Rev. Phys. Chem.* **33**, 353 (1982).
- <sup>73</sup>V. Khidekel, V. Chernyak, and S. Mukamel, *J. Chem. Phys.* **105**, 8543 (1996).
- <sup>74</sup>M. Cho, N. F. Scherer, G. R. Fleming, and S. Mukamel, *J. Chem. Phys.* **96**, 5618 (1992).
- <sup>75</sup>A. A. Abrikosov, L. P. Gorkov, and I. E. Dzyaloshinski, *Methods of Quantum Field Theory in Statistical Physics* (Dover, New York, 1975).
- <sup>76</sup>C. K. Chan and J. B. Page, *Chem. Phys. Lett.* **104**, 609 (1984).